ABSTRACT

WANG, JINGMEI. Antimicrobial Finishing of Hernia Mesh with Carboxymethyl Chitosan. (Under the direction of Martin W. King).

The current treatment for ventral, inguinal or umbilical hernia repair is using an implantable mesh to reinforce the abdominal wall without tension. The most commonly used meshes are made from synthetic materials such as polypropylene (PP), polyester (PET) and expanded polytetrafluorethylene (ePTFE). Synthetic meshes are chemically stable, biocompatible, and have adequate mechanical strength that does not deteriorate with time. However, the post-operative or late infection rate for open surgical repair that involves a mesh is 6% ~ 10%. And the infection not only brings suffering to the patient and additional costs to the healthcare system, but also may require the removal of the mesh during a re-operation, which can lead to other complications.

Therefore, the main objective of this study was to identify and evaluate the effectiveness of applying a surface treatment to a synthetic hernia mesh that will prevent localized bacterial infections. In this study carboxymethyl chitosan (CMC) was selected as a potential antimicrobial agent that could either be chemically grafted and cross-linked or coated onto a commercially knitted polyester hernia mesh without changing the mesh's mechanical, handling and suturing properties. CMC is derived from chitin, which is obtained from shell-fish, and is known for its hemostatic and antimicrobial properties.

By first exposing the polyester fibers to radio frequency plasma under an oxygen-rich atmosphere, the surface was activated by the generation of oxygen containing groups, which were able to react with CMC and its cross-linking agent, citric acid. Chemical elemental analysis confirmed that the

CMC was successfully cross-linked to the PET surface. After a certain level of CMC concentration, the cross-linking efficiency was not advanced further, and the morphology of the polyester fiber surface did not appear to change. In terms of the antimicrobial performance neither the CMC chemically cross-linked treatment nor the application of the plasma treatment before the CMC cross-linking displayed any positive antibacterial performance against *E. coli* or *S. aureus* strains of bacteria. And the mechanical properties of both groups, as measured in terms of their bursting strength, were reduced as a result of the chemical grafting and crosslinking, and the cross-linked physical coating.

Antimicrobial Finishing of Hernia Mesh with Carboxymethyl Chitosan

by
Jingmei Wang

A thesis submitted to the Graduate Faculty of
North Carolina State University
in partial fulfillment of the
requirements for the degree of
Master of Science

Textile Engineering

Raleigh, North Carolina

2018

APPROVED BY:

_____	_____
Dr. Martin W. King Committee Chair	Dr. Wendy E. Krause

_____
Dr. Ashley C. Brown

DEDICATION

To my beloved family

To my friends

To my advisor Dr. Martin W. King

BIOGRAPHY

Jingmei Wang was born on November 20th, 1995 China. She received her bachelor's degree in Textile Engineering in June 2017 from Donghua University, Shanghai, P.R. China. She was luckily accepted into an exchange program between Donghua University and North Carolina State University for further study in 2016. She joined in Dr. King's biomedical textile research group and continued her study in biomedical textile materials. She is expected to receive her master degree in December 2018, and plans to look for a career in biomaterials after her graduation.

ACKNOWLEDGMENTS

I would like to give me sincere gratitude to those who have helped me in the research. First, I want to give my deepest appreciation to my advisor Dr. Martin W. King for providing me such a great opportunity to work in the area of hernia mesh that I am interested in and it is an honor to work with him in the past two years. His dedication on research and pursuit for new knowledge are always inspiring and motivating me. Thanks to his support and encouragement, this project could progress successfully. Moreover, his passion for work and life inspires me and all the students in his group.

I also want to appreciate other members in my advisory committee. Many thanks to Dr. Krause and Dr. Brown. They agreed to be my committee and shared their valuable knowledge and expert opinions during my study. I also appreciate the support given by Dr. Hudson. He gave some valuable knowledge of chitosan. And I also wish to address special thanks to Dr. Bernacki for allowing to use her research facility and lending her expertise with bacteria cultures. Many thanks go to Dr. Ahmed El-Shafei for letting me use the plasma lab.

A special thanks to Birgit Anderson, Phillip Strader , Chuck Mooney, Fred Stevie and Shahriar Salim for assisting and lending their special expertise in using various pieces of laboratory equipment for research purposes.

I would also like to give my special thanks to Jialong Shen, Yu Xie, Jiyang Chen, Fan Zhang and Daxian Zha for their kind assistance and dedication with my experimental work. My appreciation also goes to all the group members in Biomedical Textile research group. It is their valuable advice

and experience in the area that helped me to complete this project. I am especially thankful to Yu Xie, Jialong Shen and Jiyang Chen for spending their time to assist me with my experimental work.

Last but not the least, I would like to express my deepest appreciation to my family for their everlasting love and belief in me, and I really appreciate them for their understanding and respect for my decisions. My appreciation also extends to all my friends in Raleigh and in China who has given me such extensive support and encouragement.

TABLE OF CONTENTS

LIST OF TABLES

LIST OF FIGURES

CHAPTER 1. INTRODUCTION

1.1 Background

An abdominal wall hernia is a weakness, defect or rupture of the abdominal wall that enables the intestines or other organs to protrude through the opening. An estimated 20 million hernias are surgically repaired every year in the world (Zöller, Ji, Sundquist, & Sundquist, 2013). Abdominal wall hernias can be classified into different types depending on their location and size. They include ventral, inguinal, umbilical and incisional hernias. Currently the recommended therapy is to implant a mesh to cover the defect and reinforce the abdominal wall without tension, This approach does not induce additional pressure in the tissue around the hernia and so reduces the risk of recurrence compared with the alternative tissue closure techniques (Dominguez, Gonzalez, & Donkor, 2015; Beard et al., 2016). A hernia mesh is usually used to repair hernia defects larger than 74 cm^2, and the types of materials that are used can be divided into synthetic, bioprosthetic and biodegradable meshes. Synthetic meshes are currently the most common repair material used for the reinforcement of ventral and other abdominal wall hernias, due to their superior mechanical properties, inert chemistry, biocompatibility and their ability to be sterilized. Additionally, most synthetic materials are not biodegradable, and will stay in the body permanently.

However, potential complications follow the implantation of such synthetic meshes. Such complications include early and late infections, perforation of the abdominal wall, the formation of seromas, groin pain, mesh adhesion to neighboring tissue and organs and recurrent hernias (Conze et al., 2005; Reilingh et al., 2003). The post-surgical infection rate for ventral hernias treated laparoscopically occurs between 0% ~ 3.6%, while for open repair employing an

implantable mesh the infection rate jumps to 6% ~ 10% of cases. If the surgical site becomes infected, it is possible for the mesh to be salvaged with local wound treatment and antibiotics. However, if a regime of medication is not effective in controlling an early or late infection, then is necessary to remove a synthetic mesh in a follow-up operation. Because the patient needs to be repaired again and receive another mesh implant, this adds cost, time and an additional burden to the patient and the healthcare system. When infection occurs, the most common micro-organism is *Staphylococcus aureus (S. aureus),* which is a Gram positive bacteria found in up to 81% of cases. On the other hand, Gram negative micro-organisms have also been implicated in up to 17% of mesh infections. (Butler et al., 2013). In recent years, the application of novel coatings on light-weight meshes is a new development to prevent post-surgical mesh adhesions and early and late bacterial infections (Sanbhal et al., 2017).

1.2 Goals and Objectives

The goal of this study is to apply an antibacterial agent to a synthetic hernia mesh using a surface modification technique that imparts antibacterial activity without changing the mechanical, handling and suturing properties of the mesh. The antibacterial agent needs to be biocompatible, safe and non-toxic. And the use of the chitosan derivative, carboxymethyl chitosan, was proposed as the antibacterial agent. It can be grafted and cross-linked to synthetic substrates by a plasma surface modification and/or by chemical cross-linking. This study will also determine the effect of the plasma treatment on the cross-linking efficiency of carboxymethyl chitosan and explore the concentration of carboxymethyl chitosan solution that achieves the best antibacterial performance without compromising the mechanical properties.

The specific objectives are summarized below:

1) To apply carboxymethyl chitosan (CMC) to the surface of a polyester hernia mesh and to chemically graft the CMC to the polyester fibers with the help of a cross-linking agent.
2) To compare the amount of chemical cross-linking that is achieved by using different concentrations of carboxymethyl chitosan.
3) To apply a radio frequency plasma treatment before the cross-linking process to determine the effectiveness of the plasma treatment on the polyester fiber surface and the cross-linking efficiency of the carboxymethyl chitosan.
4) To evaluate the crosslinking efficiency through chemical analysis.
5) To evaluate the mechanical properties in terms of bursting strength of the untreated control mesh sample compared to the carboxymethyl chitosan physically coated and crosslinked sample and the plasma treated and CMC chemically grafted and cross-linked sample.
6) To evaluate the antimicrobial properties of the treated hernia mesh samples against both Gram negative and Gram positive micro-organisms, and compared them with the untreated control sample so as to determine the optimum treatment in terms of antimicrobial performance.

1.3 Outline of the Thesis

This thesis consists of five chapters. The first chapter provides a brief introduction to the concept of hernia defects and how meshes are used for their repair. It also lists the goals and objectives of the study. The second chapter reviews the literature describing the anatomy and pathology of abdominal wall hernias, and describes the use of hernia meshes for current surgical repair. It specifically presents information about the structure and properties of chitosan and its derivatives, and describes how surfaces can be modified by the plasma, cross-linking and grafting methods

used in this study. The third chapter introduces the specific experimental details, including the chemical characterization and measurement of the mechanical properties and antimicrobial performance of the mesh samples after surface treatment. The fourth chapter presents the experimental results and discusses the findings in terms of surface morphology, chemical characterization and mechanical and antibacterial properties. The last chapter summarizes the results, revisits the goals and objectives so as to draw conclusions about the project. It also gives recommendations for future study.

CHAPTER 2. LITERATURE REVIEW

2.1 Anatomy of the Abdominal Wall

Abdominal wall surgery relies on a thorough understanding of all the components of the abdominal wall, as well as their function and physiology. The abdominal wall is composed of a midline and anterolateral group of muscles comprising four main paired muscle layers as well as a paired fifth muscle group. The muscular group layers are covered by subcutaneous fat and skin and superficial neurovascular structures. The rectus abdominis and the pyramidalis muscles comprise the midline group. The bilateral anterolateral groups are composed of a trilaminar structure consisting of the external oblique muscles (EOMs), the internal oblique muscles (IOMs), and the transversus abdominis muscles (TAMs) (Figure 2.1). When repairing or reconstructing an abdominal wall defect, not only are the muscular components of crucial importance, but the restoration of the linea alba is also a goal of abdominal wall reconstruction (Novitsky, 2016).

2.1.1 Linea Alba

The linea alba (Figure 2.1) is a completely fibrous structure composed of collagen and elastin. It reaches from the xiphoid process to the pubic symphysis and provides an inferior triangular reinforcement to the muscle wall. Above the umbilicus, the linea alba is wide and thin; below the umbilicus, it is narrow and thick. The width varies among different populations, with the widest observation at 3 cm above the umbilicus varies from 6 to 22 mm (Beer et al., 2009). The clinical function of the linea alba is to support the abdominal muscles, particularly the rectus muscles. Without the fibrous properties of the structure there is a lack of muscle tone which leads to

weakness and the formation of the majority of de novo ventral hernias. Additionally, since most intra-abdominal access occurs via a midline laparotomy, the linea alba is also the location of most iatrogenic hernias. Then, in order to reconstruct the abdominal wall, the paired rectus muscles need to be brought back to the midline to restore the linea alba (Novitsky, 2016). When measuring its biomechanical performance, the linea alba provides the nonlinear elastic, anisotropic force-elongation behavior of the human abdominal wall (Förstemann et al., 2011). As a result, the surgical technique used can significantly affect the result. For example, when closing wounds laparoscopically, patients can not only benefit from the use of larger bite depths and smaller bite separations, but also from lateral incisions and the insertion of sutures longitudinally (Cooney et al., 2017).

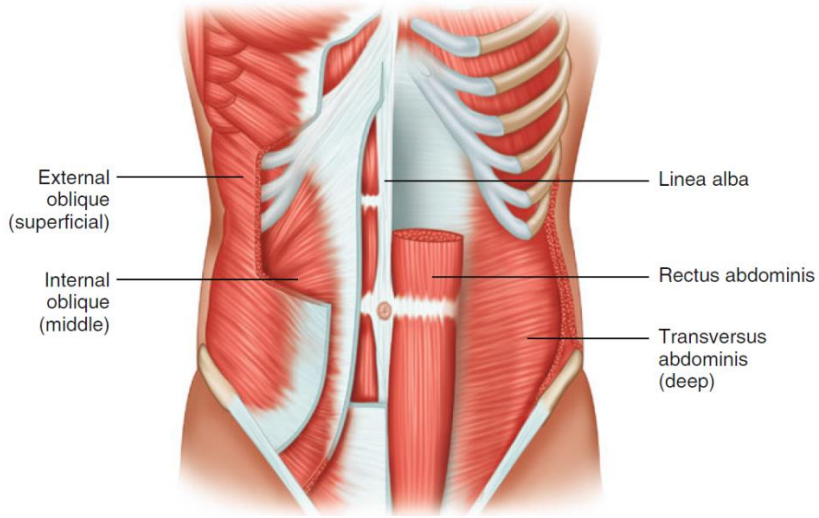

Figure 2.1 Muscles of the abdominal wall (Novitsky, 2016).

2.1.2 Midline Muscular Group

The midline group is comprised of the rectus abdominis and pyramidalis muscles (Figure 2.2). The rectus abdominis (Figure 2.1) is an anterior abdominal muscle divided into two vertical muscle

components by the linea alba. The rectus abdominis originates at the pubic crest and the pubic symphysis, and extends to the costal cartilage of the fifth, sixth, and seventh ribs. It is innervated by the lower six thoracic intercostal nerves. The rectus abdominis is the main trunk flexor of the body and also serves as an accessory muscle for respiration by pulling the ribs downward, which increases the volume of the chest cavity (Cruz & Mautner et al., 2016). The vascular supply to the rectus muscles is different from the anterolateral group, and in the event of damage to the relevant neurovascular perforating bundles during surgery, this can lead to atrophy of the rectus complex, and should be avoided if possible. So, preservation of the neurovascular supply leads to the maintenance of native rectus abdominis function and thus a more robust and functional repair (Novitsky, 2016).

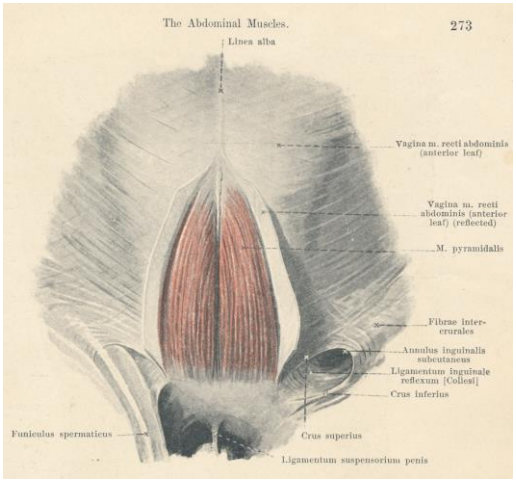

Figure 2.2 Pyramidalis muscles (Landuyt, Hamdi, Blondeel, & Monstrey, 2003).

The pyramidalis muscles are small triangular-shaped muscles that are located on the lower side between the surface of the rectus abdominus and the rectus sheath. The location, size and symmetry of these muscles can vary a lot, and there is no significant gender predominance (Das, 2017). The precise function of pyramidalis muscles is not clear, but it's thought to add tension to the linea alba

(Lovering & Anderson, 2008). Due to these characteristics, the pyramidalis muscles are sometimes transferred surgically to repair small chronic wounds in the foot or ankle (Landuyt et al., 2003).

2.1.3 Anterolateral Muscular Groups

The bilateral anterolateral groups of muscles (Figure 2.1) are composed of a trilaminar layered structure (Figure 2.3), which includes the innermost transversus abdominis muscles (TAMs), the internal oblique muscles (IOMs), and the external oblique muscles (EOMs).

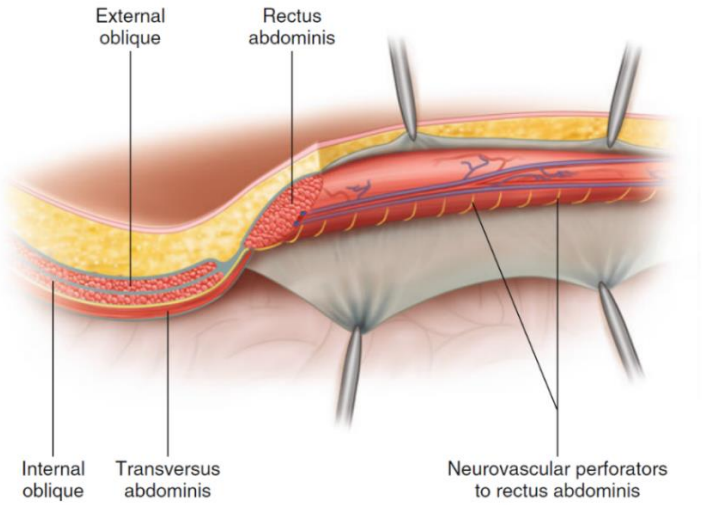

Figure 2.3 Cross section of the anterior abdominal wall (Novitsky, 2016).

The transversus abdominis muscle (TAM) fibers originate from the inner surfaces of the 7^{th} to 12^{th} costal cartilage, the anterior leaflet of the thoracolumbar fascia, the iliac crest, and the lateral third of the inguinal ligament. They are oriented in the horizontal direction until they become inserted into the linea alba, the pubic crest, and the pectineal line. At this point they interdigitate with those of the diaphragm, and in the lower region, there is a significant aponeurotic component to the muscle. The internal oblique muscle (IOM) fibers originate from the anterior leaflet of the thoracolumbar fascia, the anterior two-thirds of the iliac crest, and the lateral half of the inguinal

ligament. They are oriented in a superomedial manner and inserted along the inferior border of the 10^{th} – 12^{th} ribs and the linea alba. The external oblique muscle (EOM) fibers originate from the external surface of the 5^{th} – 12^{th} ribs, and are attached to the linea alba and pubic tubercle, and anteriorly to the iliac crest (Novitsky, 2016). Except for the origin and the orientation of the muscle fibers, there are regional differences in their thickness (Table 2.1) and fascicle length (Table 2.2). For example, their thickness is about 1.3 mm in the upper region; the TAM muscle thickness becomes thinner around 0.7 mm in the middle and lower region, whereas the IOM lower and middle regions become thicker around 1.8 mm (Urquhart, Barker, Hodges, Story, & Briggs, 2005).

Table 2.1 Mean and (standard deviation) of muscle thickness for regions of TAM, IOM and EOM (n = 24) (Urquhart et al., 2005).

Region	**Muscle thickness**		
	TAM	**IOM**	**EOM**
Upper	**1.2 (0.4)**	**1.3 (0.5)**	**1.4 (0.5)**
Middle	**0.7 (0.2)**	**1.8 (0.9)**	**1.7 (0.8)**
Lower	**0.7 (0.3)**	**1.9 (0.7)**	

Table 2.2 Mean and (standard deviation) of fascicle lengths for regions of TAM, IOM and EOM (n = 24) (Urquhart et al., 2005).

Region	**Fascicle length**		
	TAM	**IOM**	**EOM**
Upper	**9.0 (1.2)**	**8.8 (2.3)**	**10.6 (2.4)**
Middle	**11.3 (1.5)**	**10.8 (2.4)**	**18.4 (0.8)**
Lower	**3.6 (1.1)**	**5.7 (1.1)**	

Functionally, The TAM works with posterior fibers of the IOM to form a “corset” around the visceral sac and this could provide a hoop tension by their synergistic action (Novitsky, Elliott, Orenstein, & Rosen, 2012). Except for the circumferential tension by IOM, it also works with EOM on the contralateral side to provide ipsilateral rotation and torsion of the trunk (Novitsky, 2016).

2.2 Classification of Hernias

The abdominal wall hernia (AWH) is a weakness, rupture or defect in the abdominal wall which allows the intestines and other organs to protrude through the opening. It is estimated that about 20 million hernias are repaired every year in the world. Despite the fact that there are a variety of abdominal wall hernias, such as ventral, inguinal, umbilical and incisional hernias, it is the inguinal hernias that account for 75% of abdominal wall hernias which, due to the differences in male and female anatomy, are more common in men and femoral and umbilical hernias are more common in women (Zöller, Ji, Sundquist, & Sundquist, 2013). A classification for different kinds of hernias is needed to compare publications and future studies on these hernias. So in recent years, the European Hernia Society (EHS) has provided an effective classification system for clinical applications and research purposes (Muysoms et al., 2009).

2.2.1 Primary Abdominal Wall Hernias

For the primary abdominal wall hernias, location and size are the two main variables to use and location includes both two midline (epigastric and umbilical) and two lateral hernias (Spigelian and lumbar). The term “diameter” is used to determine the size. And for nominative descriptions, they are epigastric, umbilical, small, medium and large (Table 2.3) (Muysoms et al., 2009).

Table 2.3 European Hernia Society's classification of primary abdominal wall hernias (Muysoms et al., 2009).

EHS Primary Abdominal Wall Hernia Classification		Diameter cm	Small <2cm	Medium ≥2-4cm	Large ≥4cm
Midline	Epigastric				
	Umbilical				
Lateral	Spigelian				
	Lumbar				

2.2.2 Groin Hernias

Based on the Aachen classification system, the EHS developed an easier and more accurate classification system (Figure 2.4). They suggested to use the index finger as the reference of size for open surgery since the width of the fingertip is usually around 1.5~2 cm, which is similar to some surgical appliances and also easier for surgeon to use during laparoscopic surgery. The size of the hernia is defined as 1 (≤ 1 finger), 2 (1~2 fingers) and 3 (≥ 3 fingers). For the location, L means lateral, M means medial, F means femoral. For a combined hernia, it's good to mention the different locations of hernias in the table by ticking the appropriate column and row. What's more the letter P or R can be encircled to indicate a primary or recurrent hernia (Miserez et al., 2007).

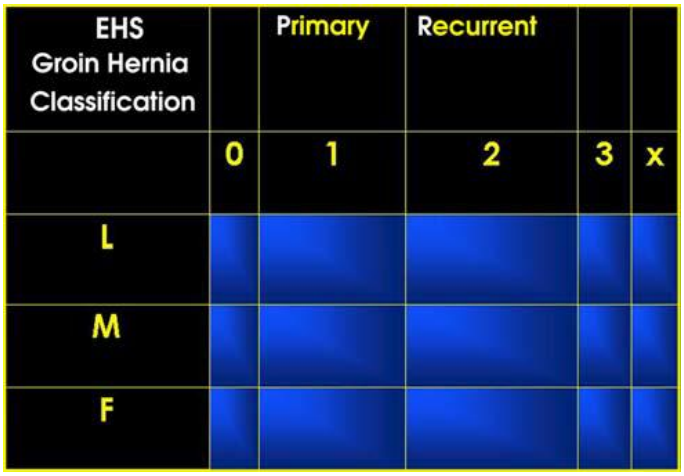

Figure 2.4 CEHS's classification of groin hernias (Miserez et al., 2007).

2.2.3 Incisional Abdominal Wall Hernias

The definition for incisional abdominal wall hernia is: Any abdominal wall gap with or without a bulge in the area of a postoperative scar perceptible or palpable by clinical examination or imaging (Korenkov et al., 2001). The abdomen is divided into two zones: the medial zone and the lateral zone. In the medial zone, they developed a memorable classification for specifying the location from M1 to M5 (Figure 2.5) from the xiphoid to pubic bone:

(1) M1: subxiphoidal (from the xiphoid till 3 cm caudally)

(2) M2: epigastric (from 3 cm below the xiphoid till 3 cm above the umbilicus)

(3) M3: umbilical (from 3 cm above till 3 cm below the umbilicus)

(4) M4: infraumbilical (from 3 cm below the umbilicus till 3 cm above the pubis)

(5) M5: suprapubic (from pubic bone till 3 cm cranially).

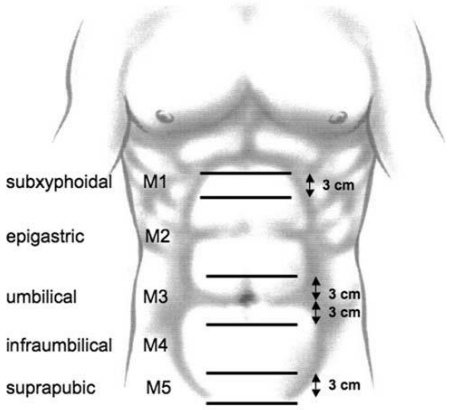

Figure 2.5 Classification for the location of medial incisional hernias (Muysoms et al., 2009).

For lateral hernias, they have identified four L zones on each side (Figure 2.6):

(1) L1: subcostal (between the costal margin and a horizontal line 3 cm above the umbilicus)

(2) L2: flank (lateral to the rectal sheath in the area 3 cm above and below the umbilicus)

(3) L3: iliac (between a horizontal line 3 cm below the umbilicus and the inguinal region)

(4) L4: lumbar (latero-dorsal of the anterior axillary line)

Incisional hernias are more complex than primary abdominal wall hernias, they have a different shape and size and may even involve multiple hernia defects. The length and width are determined so as to include the whole hernia area (Figure 2.7).

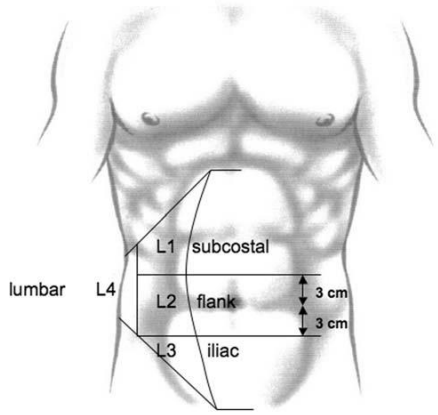

Figure 2.6 Classification for the location of lateral incisional hernias (Muysoms et al., 2009).

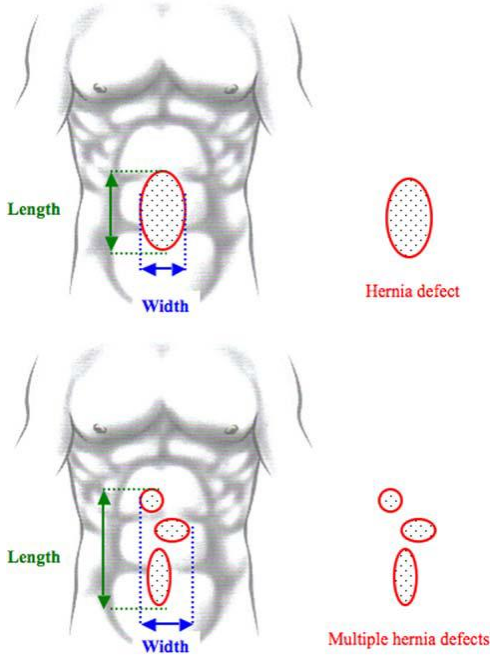

Figure 2.7 Defining the width and length of incisional hernias (Muysoms et al., 2009).

2.2.4 Parastomal Hernia

A parastomal hernia is an abnormal protrusion of the contents of the abdominal cavity through an abdominal wall defect created during the placement of a colostomy, ileostomy or ileal conduit

stoma (Muysoms et al., 2012). They have developed a new classification system based on Szczepkowski's Classification (Gil & Owski, 2011). The size of the hernia is determined by the largest dimension across the hernia orifice in any direction, and the cut-off value is 5 cm, which distinguishes between a large and small parastomal hernia. Almost half the patients have concomitant incisional hernias; so this also included in the classification system. And similar to groin hernias, there are also primary parastomal hernias or recurrences after previous treatment (Śmietański et al., 2013). In addition, subclasses of the classification were defined below:

Type I: ≤ 5 cm without incisional hernias

Type II: ≤ 5 cm with incisional hernias

Type III: > 5 cm without incisional hernias

Type IV: > 5 cm with incisional hernias

2.3 Hernia Meshes

Using a mesh to reinforce the abdominal wall without tension is generally recommended because it reduces the risk of recurrence (Dominguez, Gonzalez, & Donkor, 2015; Beard et al., 2016). A hernia mesh is commonly used for hernia defects larger than74 cm^2 and several studies have shown significantly lower hernia recurrence rates when hernia meshes are used (Breuing et al., 2010).

2.3.1 Hernia Mesh Placement

There are different configurations for placing the mesh: inter-positional, inlay and onlay. It is important to understand the difference and possible outcomes between these 3 placement locations. In recent years, the inter-positional technique has been abandoned by most surgeons owing to its high hernia recurrence rate.

Onlay repair (Figure 2.8) occurs when the mesh is placed superficially to the anterior rectus sheath and the fascia is reapproximated over the mesh. The advantage is that the mesh cannot affect the abdominal viscera directly due to the outside placement. However, several disadvantages exist: a large subcutaneous dissection is required to inset the mesh; there is an increased possibility of seroma formation; the incision would be contaminated if the incision becomes infected or there is dehiscence of the skin wound closure (Butler, Baumann, Janis, & Rosen, 2013). So an onlay mesh is commonly placed with less tension, for example, after the fascia has been closed at the midline.

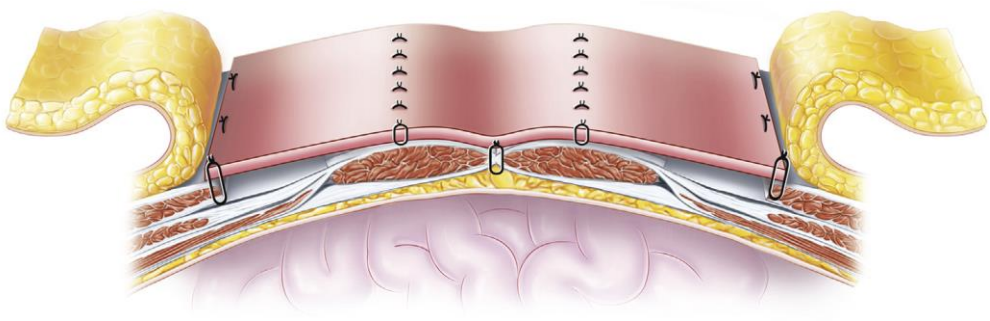

Figure 2.8 Onlay mesh placement (Butler et al., 2013).

In Europe and America, surgeons prefer an inlay mesh placement and its location could be placed in any of 3 tissue planes: intraperitoneal, retrorectus (Figure 2.9) and preperitoneal. In contrast to the onlay repair, the inlay repair can be placed with physiological tension, and the tension could spread across the abdominal wall. So, using the appropriate and safe tension across the hernia is the major goal of this technique.

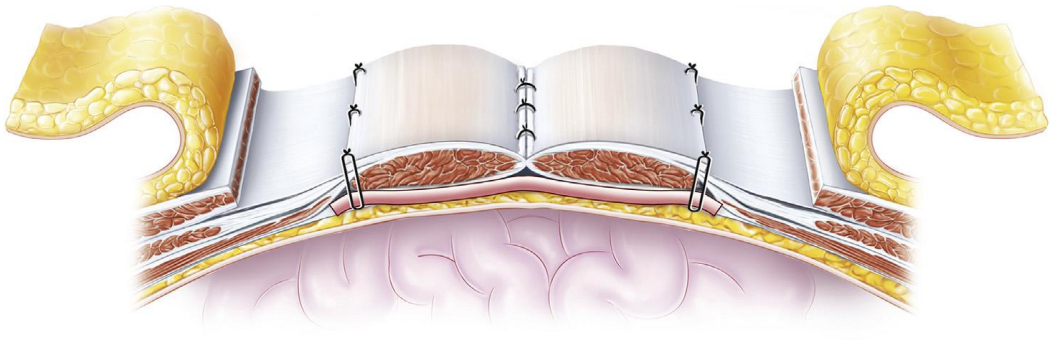

Figure 2.9 Retrorectus inlay mesh placement (Butler et al., 2013).

2.3.2 Hernia Mesh Classification

The implantation of a tension-free hernia mesh to reinforce the muscle wall or a tissue defect is recommended compared with tissue suturing techniques, because of a lower recurrence risk (Beard, Ohene-Yeboah, & Löfgren, 2016). Generally the material for fabricating the mesh is either synthetic or a natural bioprosthetic material. The ideal hernia mesh first has to meet the clinical needs (Korenkov et al., 2001). Then it has to be stable and not physically or chemically altered by tissue fluids. It must be chemically inert and prevent chemical reactions in the body. It should not generate a negative foreign body reaction, but should be non-carcinogenic, biocompatible and non-allergenic, have the physical integrity to resist mechanical strains, and to have the ability to be sterilized. Based on these general requirements, there are currently commercial synthetic, bioprosthetic and biodegradable meshes on the market.

Synthetic mesh is currently the most common repair material used for reinforcement of ventral hernias (Breuing et al., 2010) and is generally made of polypropylene (PP), polyethylene-terephtalat (PET), polytetrafluorethylene (PTFE) or polyvinylidene fluoride (PVDF) and these material is nonabsorbable which means after implanting the mesh will stay in the body

permanently. PP is a widely used material of hernia mesh and is of relatively high bending stiffness. Also, it reduced the hernia recurrences rate significantly. While, the disadvantage is the inflammatory foreign-body reaction (FBR) reported (Wang, & Zhang, 2014). PET is a member of the polyester family and it's less hydrophobic than PP. There are some advantages: minimal adhesion, less shrinkage, decreased stiffness, and better tissue incorporation. And standard polyester is mainly used in the open surgical technique (Sanbhal, Miao, Xu, Khatri, & Wang, 2017). PTFE mesh could easily cause infection and PTFE mesh must be explanted from human body because of reduced tissue incorporation and higher hernia recurrence rate (Sanbhal et al., 2017). PVDF is more resistant to degradation and hydrolysis in comparison to polyester. PVDF does not demonstrate the stiffness of filaments after in vivo implantation which is an important property of mesh for hernia repair (Klinge, Klosterhalfen, Öttinger, Junge, & Schumpelick, 2002).

For the structure of the mesh, warp knitted mesh is better than weft knitted because warp structure is easier for surgeon to cut ideal size and better structural stability (Wang et al., 2011). Secondly, heavy weight meshes are associated with increased complications and adverse events, such as fistula and adhesion formation and pain and heavyweight means increased surface area, therefore, produce a more intense FBR. So the light weight mesh always means small surface are and large pore size (Bringman et al., 2009). Thirdly, the pore size is an important parameter for hernia mesh because microporous mesh could result in better tissue in-growth and lower FBR but may lead to a higher risk of adhesions (Eriksen, Gögenur, & Rosenberg, 2007). Larger pore size provides optimal flexibility for improved physical properties, so some researchers recommended pore size like 3 and 6 mm (Bringman et al., 2009).

Table 2.4 Classification of four different categories of mesh weight (Sanbhal et al., 2017).

Mesh category	Weight (g/m^2)
Ultra-light	<35
Light	≥ 35 < 70
Standard	≥ 70 < 140
Heavy	≥140

Bioprosthetic meshes could be made from different species like human, porcine and bovine and derived from different types of tissue like dermis and pericardium, therefore, the processing method for each material is also quite different. Importantly, processing method could affect mesh properties, so researchers need to mention many processing aspects like decellularization method, crosslinking technique, extent of crosslinking, sterilization process, and packaging conditions (Novitsky, 2016). Additionally, there are some advantages over synthetic meshes, for example, their resist infection and remodel potential abilities, leaving behind host cells and native regenerated collagen. Animal studies reported a significant reduction in the strength and surface area of adhesions with the acellular dermal matrices (Butler, Baumann, Janis, & Rosen, 2013). However, recently disappointing clinical data and high cost have begun to limit its utilization (Novitsky, 2016).

Biodegradable meshes are made of synthetic absorbable filament such as polylactic acid (PLA), polyglycolic acid (PGA), poly-4-hydroxybutyrate (P4HB) and so on. These meshes could be totally absorbed after several months and the duration time depends on their processing method. And processing method works for certain functions, for example, the mesh could be multi-layers

for gradually degradation or made from co-polymers for strength requirement or special textile structure like nonwoven, knitting, woven for mechanical properties. During application, the strength will be weaker over time and finally absorbed, so the duration time is an important factor. And compared to permanent synthetic mesh, absorbable meshes have a lower recurrence rate, lower inflammatory response and also shown to have collagen deposition similar to native connective tissue (Novitsky, 2016).

2.3.2 Current Problems

There are currently several problems after the implantation of hernia repair meshes, such as mesh infection, perforation, seroma (Conze et al., 2005), groin pain, mesh adhesion and a recurrent hernia (Reilingh et al., 2003). Several factors could affect the outcome of the surgery. For example, the surgeon needs to decide the appropriate type of mesh and choose the prosthesis fixation method, whether it involves sutures, staples or tacks (Mavrodin, Antoniac, & Pariza, 2015), and also decide the surgical technique according to the individual patient requirements. What's more, early or late bacterial infections of the mesh are one of the most serious complications that can occur after ventral hernia repair. Mesh infections usually happened in 0% ~ 3.6% of laparoscopic ventral hernia repairs, and 6% ~ 10% of open repairs employing some type of mesh. The most common micro-organism infecting meshes is the gram positive bacteria, staphylococcus aureus, which is found in up to 81% of cases. In comparison, Gram negative bacteria have been implicated in only 17% of mesh infections. When infection occurs, sometimes the mesh can be salvaged with local wound treatment and antibiotics and so the mesh does not require removal (Butler et al., 2013). But if a regime of medication cannot control an infection, then the synthetic mesh will need to be removed. This means that there will be additional cost and time to the patient and burden on the

healthcare system, because the patient will need to experience a second follow-up operation. In recent years, we have seen the development of innovative coatings on light weight meshes with the objective of preventing mesh adhesion and early and late bacterial infections after implantation (Sanbhal et al., 2017).

2.4 Chitosan Derivatives

2.4.1 Chitosan

Chitosan is a linear, semi-crystalline polysaccharide, derived from partial deacetylation of a natural polymer: chitin (Figure 2.10), which is the second most abundant polysaccharide in nature after cellulose (Choi, Nam, & Nah, 2016). Chitosan (Figure 2.10) contains three reactive sites including a primary amine and two primary or secondary hydroxyl groups per glucosamine unit. As a result it is readily subject to chemical modification. The structural characteristics of chitosan mimic glycosaminoglycan components of the extracellular matrix, so the biocompatibility, biodegradability, antibacterial, hemostatic and antioxidant activities and mucoadhesive properties impart versatility (Dragostin et al., 2016).

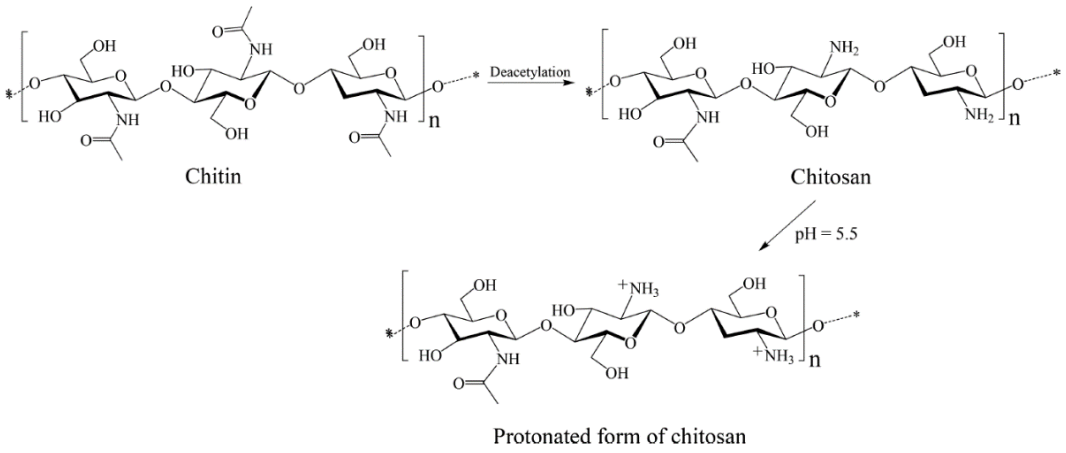

Figure 2.10 Structure of chitin, chitosan, and a protonated derivative of chitosan (Sahariah & Másson, 2017).

As an antimicrobial agent used extensively in the textile industry, chitosan has advantages over other types of disinfectants because of its superior antibacterial activity, a broader spectrum of activity, a higher killing rate and a lower toxicity towards mammalian cells. Despite all these advantages, chitosan lacks good solubility above pH 6.5. Its applications in a commercial context are not as wide as might be expected (Wang et al., 2009). Chitosan can be used to spin antimicrobial fibers or as a finishing agent for surface modification. It is only soluble in acidic solutions because the amino groups in chitosan have a pKa of ~6.5 and the antimicrobial property of the chitosan solution increases when a positively charged amine group can bind to the negatively charged bacterial surface, resulting in the disruption of the cell membrane and an increase in its permeability. Chitosan can also interact with the DNA of micro-organisms to prevent protein synthesis (Simoncic & Tomsic, 2010). But when the pH of a solution is above 6.5, not only is the solubility of chitosan problematic, but also the antimicrobial activity is less effective. So researchers are exploring chitosan derivatives that are soluble in water over a wide pH range for expanding the chitosan applications.

2.4.2 Chitosan derivatives

Given that chitosan does not dissolve in aqueous media at neutral and alkaline pH's and its antimicrobial activity likewise is not particularly good in neutral or alkaline solutions, so there is much justification to chemically modify chitosan so as to attract more interest among researchers to improve its solubility and widen its applications. Recent researchers reported that chitosan derivatives have better water solubility, antibacterial and antioxidant properties (Alves & Mano, 2008). Chitosan can be modified to include quaternary ammonium groups, alkyl and aromatic groups, substituents having free amino or hydroxyl groups, carboxyalkyl groups and amino acids

and peptides (Sahariah & Másson, 2017). And different applications have been found for these chitosan derivatives. Chitosan derivatives could not only be used in biomedical applications, such as drug delivery, tissue engineering and antimicrobial agents, but also in absorption of metal ions and dye removal (Alves & Mano, 2008).

2.4.3 Carboxymethyl Chitosan

Carboxymethyl chitosan (CMC) is one of the chitosan derivatives synthesized by introducing carboxymethyl to the chitosan structure. CMC can drastically increase the solubility of chitosan at neutral and alkaline pH values without affecting their characteristic properties. In addition, CMC has superior antimicrobial activity, biocompatibility and safety for humans. Generally, there are O-CMC, N-CMC, N, singlet O and N,N-dicarboxymethyl chitosan which have different chemical structures (Figure 2.11). For antimicrobial properties, the antimicrobial activity of different types of CMC against *E. coli* was found to increase by converting NO-CMC < Chitosan < O-CMC because of the reduced number of protonated amino groups in NO-CMC (Upadhyaya, Singh, Agarwal, & Tewari, 2013). And against *S. Aureus*, O-CMC and N also have improved antimicrobial properties (Anitha et al., 2009). In addition to its antimicrobial performance, CMC performs well enhancing antioxidant activity and apoptosis inhibitory activity. And due to its superior properties compared to chitosan, CMC can be used in biomedical and pharmaceutical applications. For example, in wound healing applications, NO-CMC could promote the proliferation of skin fibroblasts and significantly reduce adhesion formation and re-formation (Upadhyaya et al., 2013). In tissue engineering applications, CMC readily forms hydrogels and its degradation properties make it a suitable scaffold material for new tissue generation because it minimizes the inflammatory response and limits toxic degradation by-products. CMC can be

mixed with gelatin and hydroxyapatite to provide an injectable gel to treat irregular small bone defects (Mishra et al., 2011). In drug delivery, CMC based systems can be used to deliver anti-cancer drugs, anti-inflammatory drugs, proteins/ peptides and vaccines, and CMC can also be used in targeted drug delivery (Upadhyaya et al., 2013).

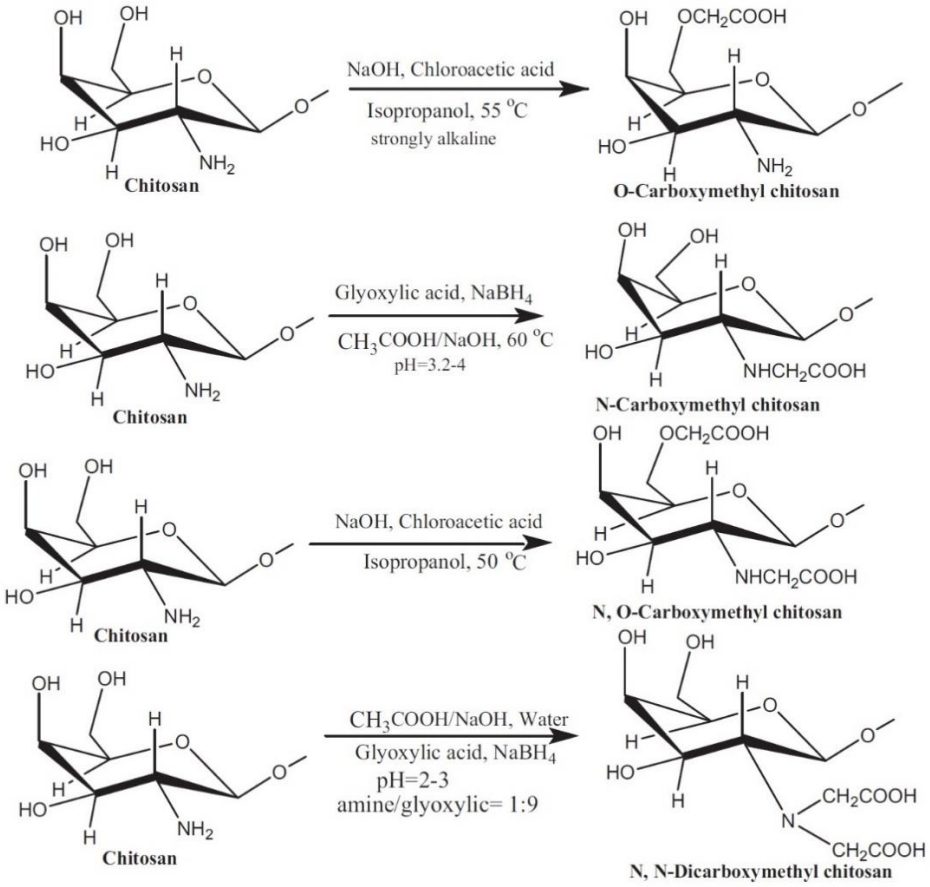

Figure 2.11 Carboxymethyl Derivatives of Chitosan (Upadhyaya et al., 2013).

2.5 Plasma Modification

Polymers are widely used in biomedical applications due to their versatility. For individual applications, their inherent bulk properties can be altered by a variety of surface modification methods. These surface treatments will just change the surface chemistry and morphology, which

means their bulk properties will remain unaltered (Neděla, Slepička, & Švorčík, 2017). And in general, these surface treatments include exposure to laser treatment, ion implantation, radio frequency plasma and UV-irradiation (Alonso et al., 2009).

Radio frequency plasma treatment can be applied under atmospheric pressure and also in vacuum. The radio frequency (RF) vacuum plasma is conducted under vacuum, leading to high cost and small batch sizes. On the other hand, atmospheric plasma (Figure 2.12) could induce different forms of interactions including electron and ion impact, free radical/surface interactions, surface erosion, singlet oxygen release and chemical deposition. And for textile applications, these phenomena can be used for etching, chain scission, polymerization, cross-linking, and the development of functional groups (Hwang, Matthews, Mccord, & Bourham, 2004). Plasma is considered to be the fourth state of matter due to the composition of ionized gas containing a mixture of ions, electrons, radicals and photons. When these energetic active particles collide with the polymer surface, some of the chemical bonds will break making the surface more reactive and easier to experience surface modification. Depending on the type of gas in which the plasma is generated, certain new functional groups can be grafted onto the surface (Morent, Geyter, & Leys, 2008).

The gases for RF plasma treatment can be divided into reactant gases and unreactant gases. For reactant gas, oxygen and ammonia are usually used, and the polymer material can react with different oxygen forms of oxygen plasma:

(1) Atomic oxygen reaction: $RH + O \rightarrow R\cdot + H\cdot + O_2$

$\rightarrow R_1\cdot + R_2O\cdot$

$$\rightarrow R\cdot + OH\cdot$$

(2) Oxygen molecules reaction: $R\cdot + O_2 \rightarrow ROO\cdot$

(3) Superoxide free radical reaction: $ROO\cdot + R'H \rightarrow ROOH + R'$

Similar to oxygen, nitrogen plasma includes N, N^+, N^-, N^M (metastable state), N*, N_2*. So there are many active species to participate in the reaction. Some of the species bond to macromolecular chains by reacting with free radicals and unsaturated bonds on the surface of the material. For the unreactant gas, Ar, He and H is used to create and stabilize the RF plasma. It can transfer surface energy and stabilize the large number of free radicals that are produced on the material's surface. And as a result, the free radicals formed in the material's surface produce a crosslinked structure (Yu et al., 2016). For example, graphene and graphene nanoribbons receive different types of etching after hydrogen treatment (Xie, Jiao, & Dai, 2010). And PET fabric generates oxygen based functional groups like hydroxyl and carboxylic groups on its surface after plasma treatment with a helium and oxygen gas mixture (Shin et al., 2006).

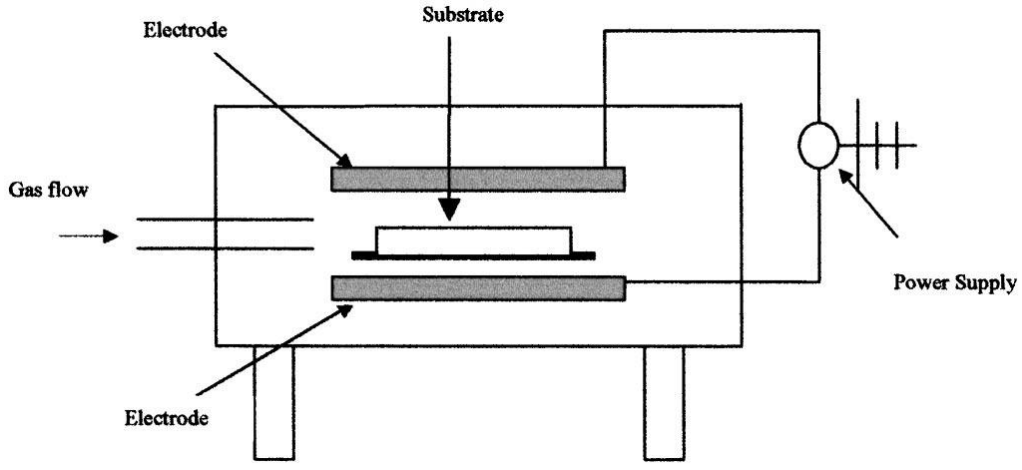

Figure 2.12 A schematic diagram of an atmospheric pressure plasma system (Hwang et al., 2004).

2.6 Grafting and Crosslinking

2.6.1 Definition

Grafting is an effective surface modification method, which is described as covalent and irreversible attachment. The process can be accomplished by either “grafting to” and “grafting from” (Figure 2.13). “Grafting to” means unfunctionalized monomers react with the backbone polymer to form the grafted product, and “grafting from” is achieved by treating a substrate with some method to generate immobilized initiators followed by polymerization (Bhattacharya, Rawlins, & Ray, 2009). For “grafting from” methods to form active sites, free radicals and/or ions are needed, including UV light, low temperature RF plasma treatment, wet chemical treatment, ozone activation and so on (Yu et al., 2016). On the other hand, crosslinking is the association of polymers through a chemical covalent or ionic bond. It is also irreversible. Generally it can be intramolecular and intermolecular.

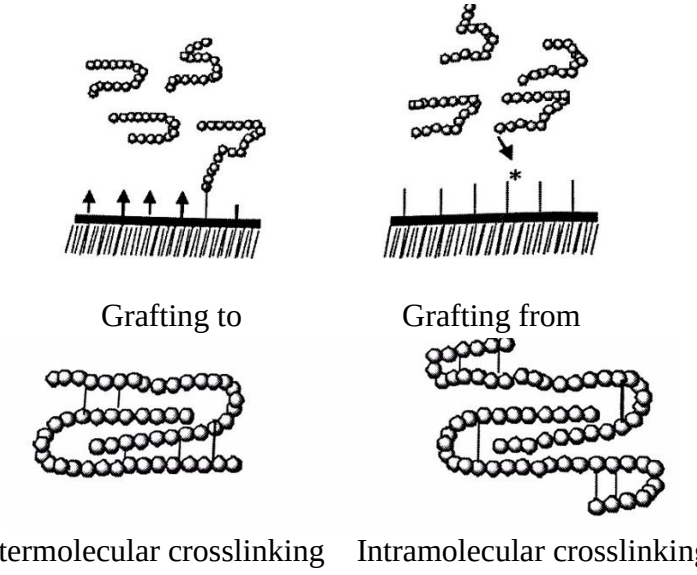

Figure 2.13 Schematic diagram of grafting and crosslinking (Bhattacharya et al., 2009).

2.6.2 Grafting Classification

The grafting and crosslinking reactions can be performed by different pathways that could be chemically or radiation driven. Chemical methods include redox reactions, living radical formation and ionic grafting. The redox reaction is the conventional one to produce free radicals. Some probable reaction pathways include Fenton's reagent (Fe^{2+}/H_2O_2), Fe^{2+}/persulphate, Fe^{2+}/hydroperoxides, direct oxidation and so on. Some of them are not used very often in the crosslinking reaction. Examples, such as Fenton's reagent and other reactions are listed below (Bhattacharya et al., 2009):

(1) Fenton's reagent: $H^2O^2 + Fe^{2+} \rightarrow HO\cdot + OH^- + Fe^{3+}$

$$HO\cdot + \text{Polymer} \rightarrow H_2O + \text{Polymer}\cdot$$

(2) Fe^{2+}/Persulphate: $S_2O_8{}^{2-} + Fe^{2+} \rightarrow SO_4{}^{-\cdot} + Fe^{3+} + SO_4{}^{2-}$

$$SO_4{}^{-\cdot} + H_2O \rightarrow HSO_4{}^- + OH\cdot$$

$$HO\cdot + \text{Polymer} \rightarrow \text{Polymer}\cdot + H_2O$$

(3) Fe^{2+}/Hydroperoxides: $t-BuOOH + Fe^{2+} \rightarrow t-BuO\cdot + OH^- + Fe^{3+}$

$$t-BuO\cdot + \text{Polymer} \rightarrow t-BuOH + \text{Polymer}\cdot$$

Radicals are involved in free-radical grafting and ionic grafting. For free-radical grafting, the irradiation of macromolecules can cause homolytic fission and free radicals are formed from the fission byproducts and attach to the polymer. Under radiation, the initiator is not essential, while the medium is important. If irradiation is carried out in air, peroxides may be formed on the polymer and the active lifetime of these free radicals depends on the nature of the polymer. There are three different ways that grafting can occur: (a) pre-irradiation (b) peroxidation and (c) the mutual irradiation technique. In the pre-irradiation technique, the polymer is first irradiated in

vacuum or in an inert gas to form free radicals. The irradiated polymer substrate is then treated with the monomer, in liquid, vapor or as a solution in a suitable solvent. In the peroxidation grafting method, the long chain polymer is subjected to high-energy radiation in the presence of air or oxygen. The stable peroxide products are then treated with the monomer at higher temperature. Then when the peroxides undergo decomposition to radicals, they initiate grafting (Bhattacharya, 2004). The possible mechanisms are described below (P is Polymer and M is Monomer):

(a) $\text{Pre} - \text{irradiation:} \quad \text{P}\sim\text{P}^{\cdot} + \text{M} \rightarrow \text{PM}.$

(b) $\text{Peroxidation:} \quad \text{P} \overset{\text{O2}}{\rightarrow} \text{P} - \text{O}^{\cdot} + \text{OH}^{\cdot} \text{ or } 2\text{P} - \text{O}^{\cdot}.$

$$\text{P} - \text{O}. + \text{OH}. \text{or } 2\text{P} - \text{O}. - \text{M} \rightarrow \text{P} - \text{O} - \text{M}$$

(c) Mutual irradiation technique : $\text{P} + \text{M} \rightarrow \text{P}. + \text{M}^{\cdot} \rightarrow \text{P} - \text{M}^{\cdot}$

Radiation grafting can also proceed through an ionic mode, with the ions formed through high-energy irradiation. Ionic grafting may be of two different types: cationic or anionic. The polymer is irradiated to form the polymeric ion, and then reacted with the monomer to form the grafted co-polymer. The potential advantage of the ionic grafting is a high reaction rate and the formation of stereo-regular polymers. Thus, small radiation doses are sufficient to bring about extensive grafting.

In addition to chemical and radiation methods, there are also photochemical grafting, plasma grafting and enzymatic grafting methods. For photochemical grafting, when a chromophore on a macromolecule absorbs light, the structure is elevated to an excited state, which may dissociate into reactive free-radicals and the initiation of a grafting process. Also RF plasma induced free radicals have been described previously. For enzymatic grafting, the method is a new technique.

The principle is that an enzyme serves as the initiator of a chemical/ electrochemical grafting reaction (Bhattacharya, 2004).

2.6.3 Crosslinking Classification

Some methods of grafting can also be used for crosslinking, particularly when crosslinking uses a condensation method. A specific class of polymers formed through condensation reactions are known as condensation polymers. Polymers proceed through a step-by-step succession of elementary reactions between two functional groups, such as amine, alcohol, acid or isocyanate. For gelation, a three-dimensional polycondensation reaction is required with the change from liquid to solid. Then the viscous network of reactants forms pre-gels and post-gels, in which the viscosity plays an important role. Commercially crosslinked polymers that form condensation polymers via a crosslinking agent, include phenolic resins, amino resins, polyurethane resins and epoxy resin. Another polymerization technique called interfacial polycondensation requires two multifunctional reactive monomers dissolved in two mutually immiscible liquids. The polycondensation reaction therefore occurs only at the interface between the two immiscible solutions where a high molecular weight polymer is formed. For example, multifunctional aliphatic and aromatic amines in an aqueous phase and acid chlorides in an organic phase will produce a thin film which will continue to form a hollow polymer tube if the polymer is slowly drawn away from the liquid interface. In addition to these two crosslinking methods, there are interpenetrating polymer networks (IPN), simultaneous interpenetrating networks (SIN), elastomeric crosslinking and polycarboxylic acid (PCA) crosslinking (Bhattacharya et al., 2009).

2.6.4 Citric Acid

During the crosslinking process, most crosslinking agents, such as aldehydes, formaldehyde, glutaraldehyde and melamine resin, induce toxicity and are not suitable for biomedical applications. While polycarboxylic acids are a category of safe chemicals investigated for their crosslinking potential, malonic acid has been used to crosslink films of starch to improve their mechanical properties and reduce their water absorption (Dastidar & Netravali, 2012). Other polycarboxylic acids, such as malic acid, succinic acid, citric acid and 1,2,3,4-butanetetracarboxylic acid (BTCA), have all been employed to crosslink (Figure 2.14). Generally, polycarboxylic acids with more than two carboxyl groups have a better crosslinking effect than dicarboxylic acids (Shen, Xu, Kong, & Yang, 2015).

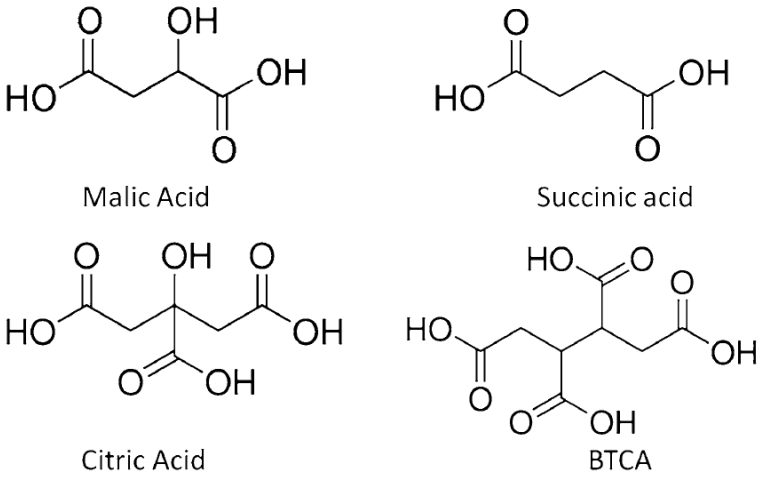

Figure 2.14 Chemical structures of polycarboxylic acids (Shen et al., 2015).

Compared with other polycarboxylic acids, citric acid is a relatively inexpensive bulk chemical derived from natural sources. Citric acid is also a food ingredient with GRAS status which means "Generally Regarded as Safe" in the US (Widsten, Dooley, Parr, Capricho, & Suckling, 2014). This makes it more attractive for food and biomedical applications. Citric acid is a safe acid that

has been widely used as an environmentally friendly and non-toxic crosslinking agent for polysaccharides, such as cellulose, chitosan (Aubert-Viard et al., 2015), and proteins like collagen (Jiang, Reddy, Zhang, Roscioli, & Yang, 2012) and wool (Hsieh, Huang, Huang, & Tseng, 2004). According to previous work, sodium hypophosphite (SHP) and similar phosphorus-based catalysts could lower the temperature required for anhydride formation by reducing the level of hydrogen bonding. It has also been suggested that catalysts such as SHP might act as buffers, shifting the pH to values low enough to promote acid-catalysis for esterification (Widsten et al., 2014). Phosphorus-based catalysts will also produce toxic decomposition gases such as phosphine if heated to their decomposition temperature of 200°C, as may happen in high-temperature curing.

So crosslinking occurred during the curing process and catalysts like sodium hypophosphite and high temperatures like 140 ~ 170°C are needed to create the reaction products (Hsieh et al., 2004):

$$\mathrm{R-COOH + HO-Chitosan \rightarrow R-CO\cdot O-Chitosan}$$

$$\mathrm{R-COOH + H_2N-Chitosan \rightarrow R-CO\cdot NH-Chitosan}$$

CHAPTER 3. MATERIALS AND METHODS

3.1 Materials

A box of three pieces (15cm x 15cm) of lightweight monofilament warp-knitted polyester hernia mesh (Parietex^{TM}) was manufactured by Medtronic Corporation (Minneapolis, MN; Cobb, Kercher, & Heniford, 2005) and supplied by Dr. Howard Levinson of Duke University Medical Center. Details about this mesh product are found at http://www.medtronic.com/covidien/en-us/products/hernia-repair/mesh-products.html. Citric acid (CA) and sodium hypophosphate (SH) were obtained from Sigma-Aldrich Corporation (St. Louis, MO). The carboxymethyl chitosan (CMC) was obtained from Santa Cruz Inc. (Dallas, TX) and the photomicrographs of the mesh were obtained at the College of Textile, North Carolina State University (Figure 3.1).

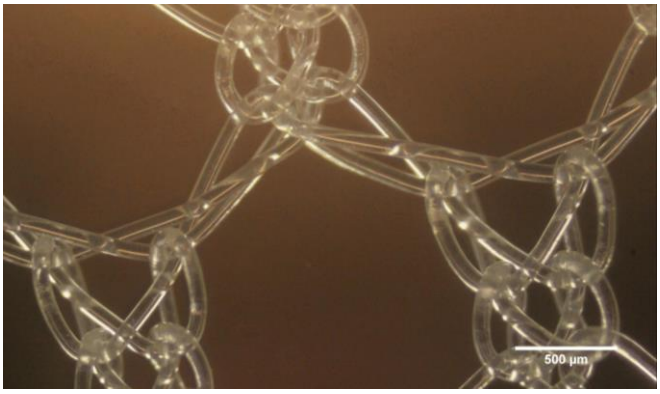

Figure 3.1 Micrograph of polyester mesh, (×40 magnification).

The warp knitted mesh fabric was first washed in 70% ethanol (Fisher Chemical) for 10 min to remove any surface impurities and then rinsed 3 times in deionized (DI) water. After the cleaning, the samples were placed on aluminum foil to dry at ambient temperature overnight, and then stored

in clean sealed plastic bags. The knitted mesh was then cut to fit the specimen size required by the specific test method.

3.2 Methods

3.2.1 Surface Modification

By referring to Aubert-Viard's work (2015), chitosan was crosslinked by citric acid (CA) onto the surface of polyester fabric, and sodium hypophosphate was used as the catalyst. Carboxymethyl chitosan (CMC) is a derivative of chitosan which contains -OH and -NH_2 groups for crosslinking. The antimicrobial performance of the CMC samples was compared between those samples with different CMC concentrations. Because plasma can activate the surface and initiate reactions between the polyester fiber surface of the mesh and the CMC/citric acid solution. Because the plasma treatment could enhance the add-on efficiency and the antimicrobial performance, so the antimicrobial test was also used to observe the effect of the plasma treatment. The CMC concentration and the plasma treatment were evaluated using FTIR and XPS along with FESEM for chemical analysis, antimicrobial performance and a standard mechanical bursting test.

3.2.1.1 CMC Crosslinking

By referring to Aubert-Viard's previous work (Aubert-Vizard et al, 2015), carboxymethyl chitosan, (CMC), citric acid (CA) and sodium hypophosphate (SH) were initially mixed together in a beaker. But because CMC and CA formed white clumps like a precipitate (Figure 3.2), it was decided to dissolve the CMC and the CA in different beakers.

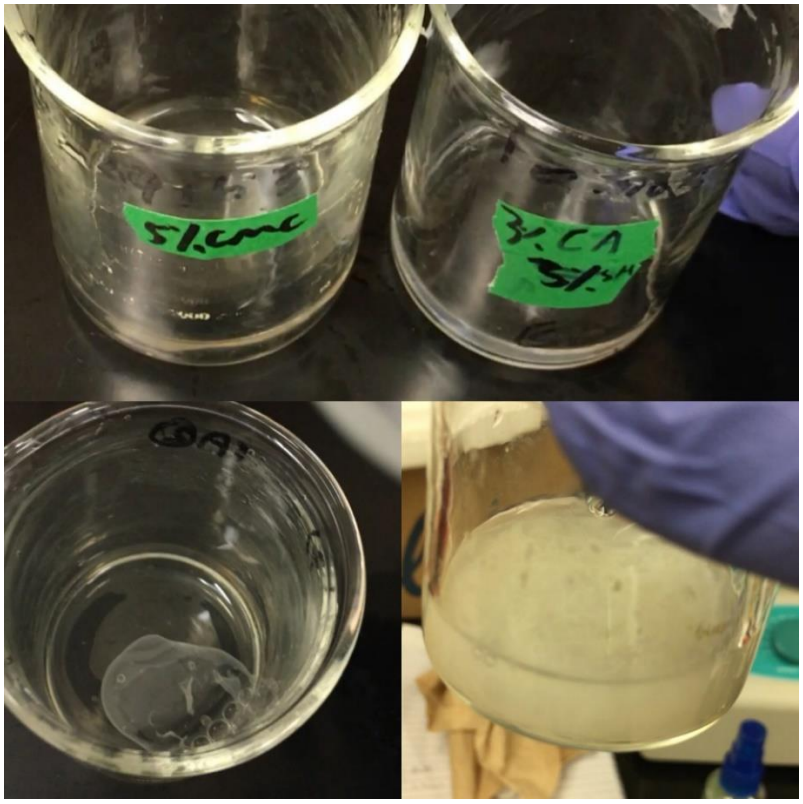

Figure 3.2 When the CA/SH solution was poured into the CMC solution a white aggregate was precipitated.

CMC was solubilized in DI water to obtain concentrations of 0.5, 1, 2, 5% wt/v by using a magnetic stirrer. Citric acid (CA) and sodium hypophosphite (SH) were dissolved together in DI water to achieve a concentration of 3% wt/v in the beaker. Then the citric acid and sodium hypophosphite were dissolved in the beaker and transferred to a spraying device. The samples were immersed in the CMC solution for 5 min and then take out and sprayed with the CA/SH solution evenly on both sides of the mesh fabric. The mesh samples were then placed on aluminum foil for curing and cross-linking at 140 ℃ for 15 min in a hot air oven (Fisher Scientific). To remove the unreacted CMC and CA, the samples were washed using DI water 3 times and then dried at 90 ℃ for 1 h. The treated samples were then wrapped in aluminum foil and stored in a zip-lock plastic bag.

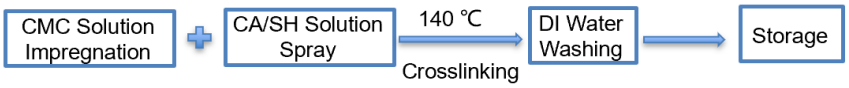

Figure 3.3 Surface impregnation and hydrolytic coating with CMC solution for preparing the CMC coated group of samples.

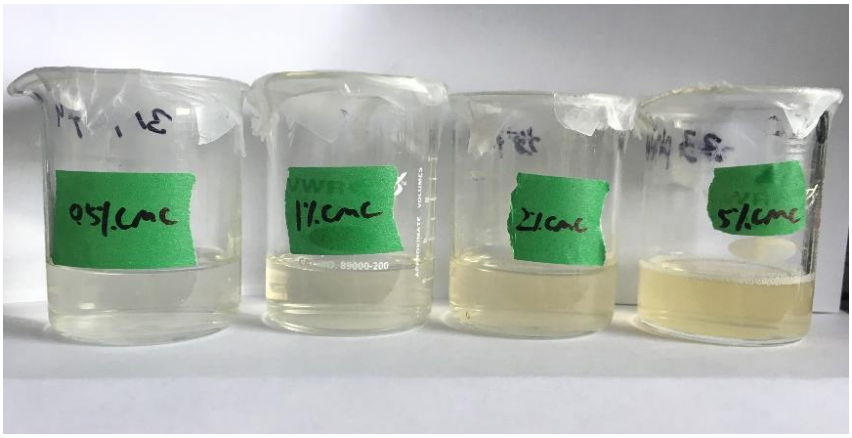

Figure 3.4 Four concentrations of CMC solution: namely 0.5, 1, 2, 5% wt/v.

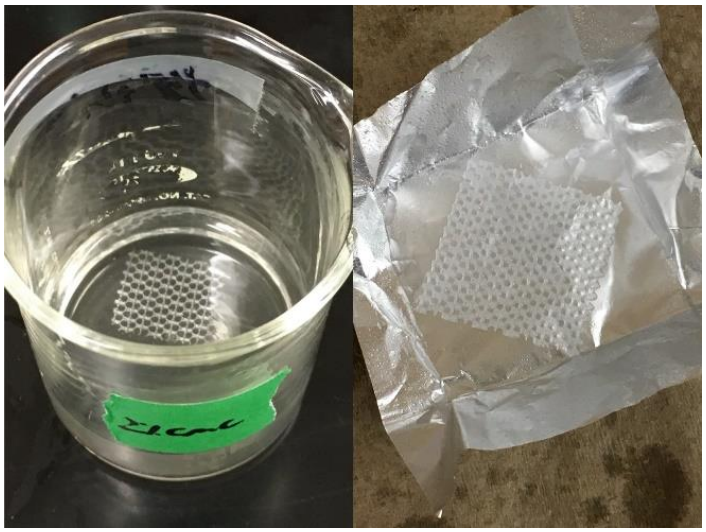

Figure 3.5 Mesh (left) immersed in CMC solution and (right) placed on aluminum foil and sprayed on both sides with CA/SH solution.

3.2.1.2 Plasma Treated CMC Crosslinking

The experimental atmospheric pressure plasma machine (Apjet Inc.) was used at the College of Textiles, North Carolina State University. A stable plasma was achieved at environmental pressure, by setting the gas flow rates at 39.6L/min for He (99%) and 0.4L/min for O_2 (1%). The energy density was 15 J/cm^2. The sample loading platform moved through the gas plasma zone (Figure3.7). So another parameter was the speed of the movement which represented the exposure time. The speed was set to be 40 cm/min and both sides of samples were plasma treated in sequence. The thickness of polyester hernia mesh was thin, so the samples were placed on the loading area without tape. After the He/O_2 plasma treatment, samples were immediately put in beakers with solutions of 0.5, 1, 2 and 5% wt/v CMC for 5 minutes. And then citric acid solution was sprayed evenly on both sides of each sample. The samples were placed on aluminum foil for curing in a hot air oven at 140 ℃ for15 min. To remove the unreacted CMC and CA, the samples were washed 3 times in DI water and then dried at 90 ℃ for 1 hour. The samples were wrapped in aluminum foil and placed in sealed plastic bags for storage.

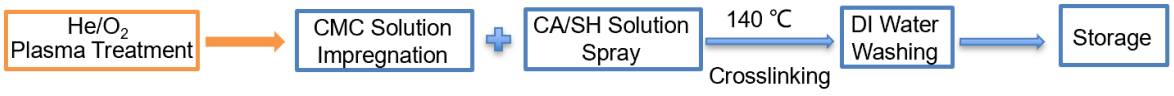

Figure 3.6 Surface treatment process for the plasma+coated group.

Figure 3.7 Environmental narrow width plasma treatment system.

3.3 Analysis Experiment

3.3.1 Surface Morphology

3.3.1.1 Field Emission Scanning Electron Microscopy (FESEM)

The surfaces of the control sample, the CMC coated sample and the plasma CMC activated sample, were observed using the FEI Verios 460L field-emission scanning electron microscope (FESEM). For surface morphological observations, the specimens were mounted on aluminum stubs with carbon tape and sputter coating with gold-palladium (60%-40%). One specimen of the plasma treated plus 1% CMC coated sample was mounted with carbon tape alone so as to evaluate the

advantage of the gold-palladium sputter coating. The samples were then placed on the FESEM sample stage (Figure 3.8) for imaging and analysis.

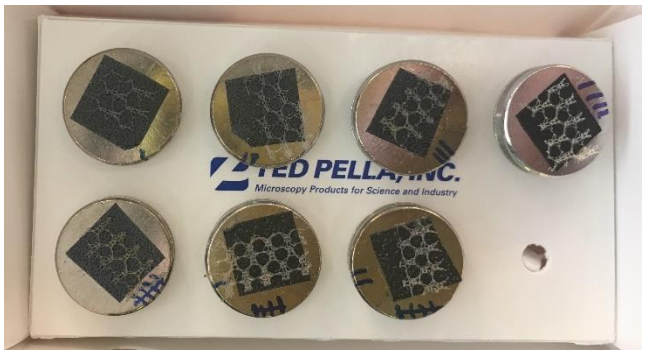

Figure 3.8 Specimens mounted on aluminum stubs with the carbon tape and sputter coated (except Specimen 4 on the top right corner).

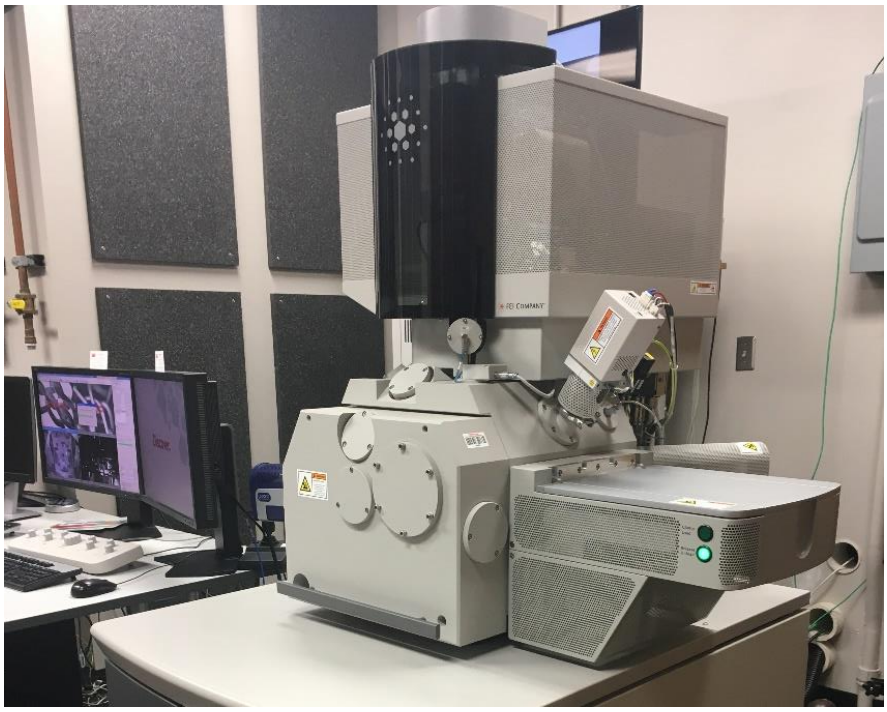

Figure 3.9 Field Emission Scanning Electron Microscopy (FESEM) system.

3.3.2 Chemistry Analysis

3.3.2.1 Fourier Transform Infrared (FTIR) Spectroscopy

Fourier Transform Infrared spectroscopy (FTIR) was used to obtain infrared absorption scans of the mesh samples using an attenuated total reflectance (ATR) attachment with a germanium crystal. Infrared spectra of the untreated control samples and the plasma treated and CMC coated samples were measured in absorbance mode between 4000 to 400 cm^{-1} wavelengths on a Nicolet Model iS50 FTIR spectrophotometer (Thermo Scientific, Madison, WI). Scanning was performed with a resolution of 4 cm^{-1}. A diamond crystal was used as part of the attenuated total reflection (ATR) attachment. The FTIR spectra were generated from an average of 64 scans, and they were then analyzed using OMNIC software (Thermo Scientific, Madison, WI) with an ATR correction to remove the absorbance of the crystal. The FTIR spectrophotometer simultaneously collected high-spectral-resolution data over a wide spectral range. Four groups of samples were analyzed: 1) the untreated control polyester mesh, 2) the polyester mesh with a plasma treatment + 1% CMC coating, 3) the polyester mesh with a plasma treatment, and 4) the 1% CMC coating without plasma, were tested and sample size for each group was a 10mm x 10mm square.

3.3.2.2 X-Ray Photoelectron Spectroscopy (XPS)

X-Ray Photoelectron Spectroscopy (XPS) is a surface analysis technique that can provide information about elemental and chemical bonding along the very top surface of a specimen (Figure 3.10). The specimen is bombarded with x-rays, and the energy of the emitted electrons is collected, measured and analyzed. The specimen needs to be totally reflective to avoid analyzing the carbon tape it is mounted on. So, the samples were cut into 1cm x 2cm pieces and placed

randomly in several layers to cover the tape and form a testable specimen. The prepared specimens were placed on the sample stage for testing (Figure 3.11).

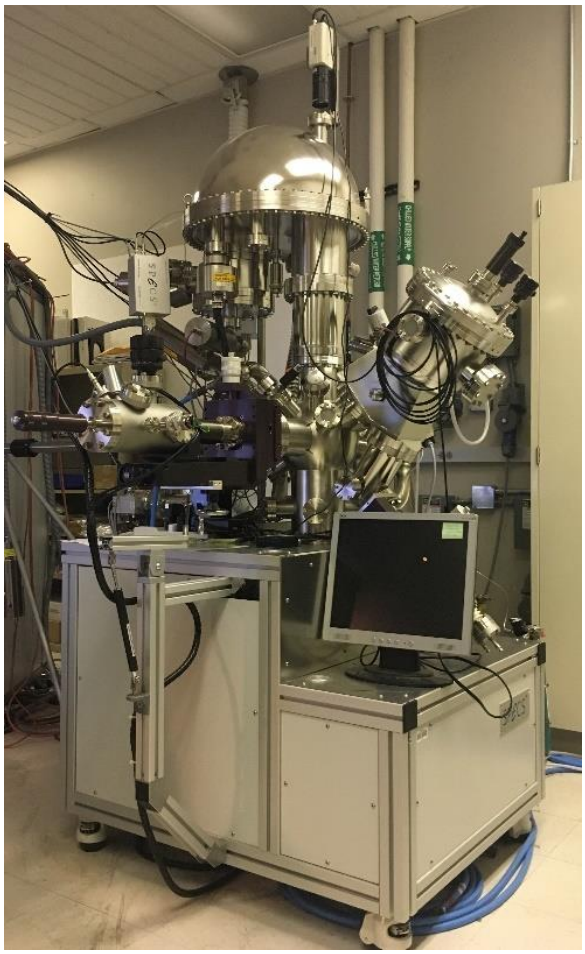

Figure 3.10 X-Ray Photoelectron Spectroscopy (XPS) system.

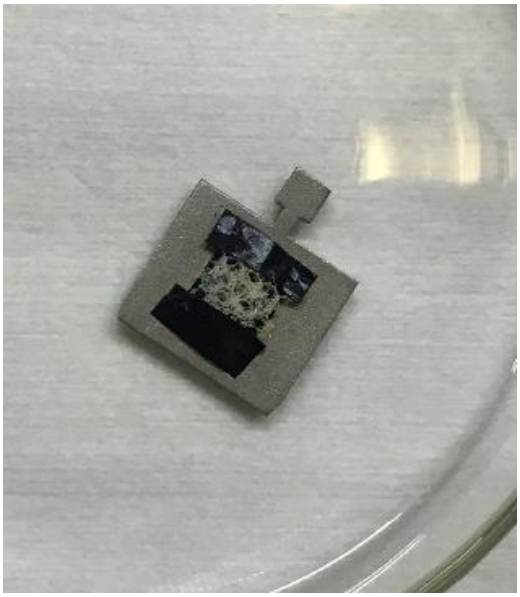

Figure 3.11 Layers of the 5% CMC coated sample mounted and ready for XPS analysis.

3.3.3 Mechanical Performance

3.3.3.1 Probe Bursting Test

The bursting strength of the hernia mesh samples was determined by the method described in ISO Standard 7198 “Cardiovascular Implants - Tubular Vascular Prostheses”. The ISO Standard 7198, was modified from the original ASTM D3787 Ball Burst Test Method. It is now used to test the mechanical properties of a range of biomedical devices requiring a square specimen size of 3cm x 3cm to fit the 2.5cm diameter specimen holder ring. The compression cage and frame were mounted on an Instron Model 5584 mechanical tester (Norwood, MA) (Figure 3.12). The square samples were clamped horizontally in the frame of the compression cage and a vertical probe with a 6mm diameter was used to create the bursting force in the center of each sample. A 2 kN load cell was used and the speed of the probe’s displacement was set at 300 mm/min, as indicated in the standard test method. The following three groups of samples were tested: the untreated control polyester mesh, the 5% CMC coated mesh and the plasma treated + 5% CMC coated mesh. And

at least 5 replicates were tested for each group. The peak load was recorded as the bursting strength and the bursting stress of each sample was calculated from the bursting force and the cross-sectional area of the probe as described in the following equation:

$$\text{Bursting Stress (MPa)} = \text{Bursting Force (N)} / \text{Area (mm}^2\text{)} = \frac{F}{2\pi r^2}$$

Where F is the peak load measured by the bursting test, r is the radius of the bursting probe (3mm) and half the area of the probe's sphere. This was because the surface area was assumed to be the contact area, since the end of the probe was half a sphere.

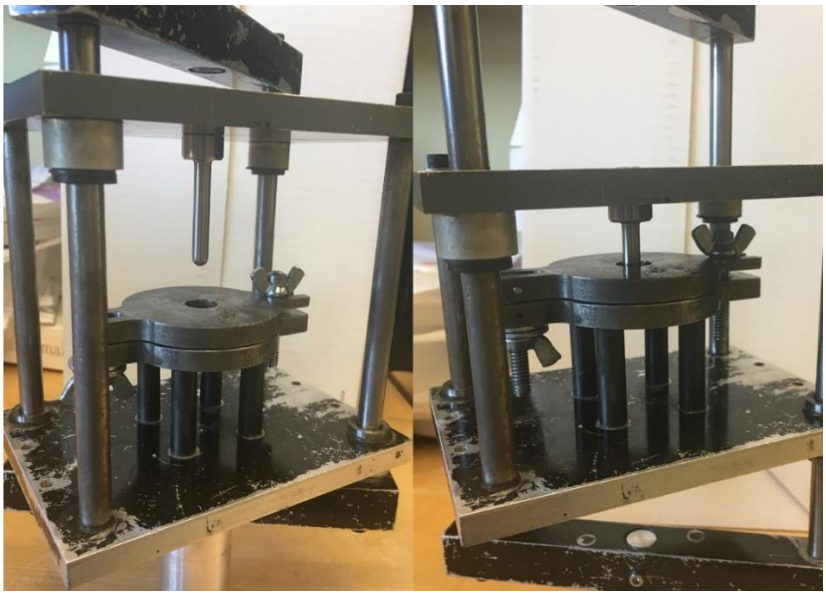

Figure 3.12 Bursting testing system showing the position of the probe (left) before and (right) after an individual bursting test.

3.3.4 Antimicrobial Test

The following antimicrobial test was used to evaluate the antimicrobial performance of the treated hernia mesh products by determining the reduction of bacterial growth and the size of the inhibition

zone for *E. coli* (ATCC 25922) and *S. aureus* (ATCC 43300) after different contact times, namely 2h, 6h and 24 hours.

3.3.4.1 Material Preparation

To culture bacteria, both triptic soy broth (TSB), a liquid medium, and triptic soy agar (TSA), a solid medium, are needed. TSA was prepared by adding 20g TSA powder and 500 ml deionized (DI) water to 500 ml glass bottle. The bottle with a loose cap was placed in an autoclave and run under steam pressure at 121 ℃ for 30 min. Because the process of increasing and decreasing the temperature and pressure each takes 30 minutes, and maintaining the steam pressure for 30 minutes, means that the autoclave cycle took a total of 90 minutes. After autoclaving, the bottle was placed in a water bath at a constant temperature of 50 ℃, and when the bottle had cooled down to 50 ℃, it was moved into the biology culture hood for pouring plates. After pouring 15ml of TSA solution into each plate, the solution became solid after cooling to room temperature, and it was then stored at room temperature for use within a week. For making the TSB medium, 15g TSB powder were added and 500 ml DI water were poured into a 500 ml glass bottle and the autoclave treatment was repeated. After autoclaving, the TSB liquid medium bottle was ready to be stored at room temperature.

Mesh samples for antimicrobial testing were cut into 8mm squares according to the antimicrobial method and washed in 70% ethanol for 10min. This was followed by rinsing 3 times in deionized water and aspirating any excess liquid with a glass tip connected to a vacuum pump and drying the samples prior to testing.

3.3.4.2 Bacteria Preparation

The two bacteria, *E. coli* and *S. aureus*, were cultured overnight following the use of an inoculation loop to inoculate the TSA plates and generate the bacteria colonies. A cotton swab was used to transfer bacteria from each of the colonies into 3ml TSB in a Tube A. The bacterial suspensions were then cultured overnight at 37 ℃ in a thermostatically controlled incubator shaker (Figure 3.13). After overnight culture, the concentrations of each bacteria in the Tube A had reached a steady state which were measured in terms of their optical density (OD) at 600nm (Figure 3.14). Then 1ml of each bacterial solution in Tube A was mixed with 2ml TSB for 2h in Tube B and the bacterial concentration increased and was counted by measuring the OD value through a known number of sequential dilutions. For dilution counting, 5 tubes of 9ml phosphate buffer saline (PBS) were prepared and labeled as Dilution Tube #1, #2, #3, #4 and #5. Then 1ml of each bacterial solution was added to Dilution Tube #1 (10^{-1} dilution) which was diluted and thoroughly mixed with PBS to make a 10ml bacterial solution. The dilution process was repeated until Dilution Tube #5. Then 100μl of each dilution was inoculated on the TSA plates, which were cultured overnight in triplicate. After culturing, those plates that contained 30 ~ 300 colonies were counted and the bacteria concentration in Tube B was calculated. After counting, when the OD value was 0.025 for *E. coli*, the TSB bacteria concentration was 1.7×10^7 CFU/ml. When the OD value was 0.026 for *S. aureus*, the TSB bacteria concentration was 2.15×10^7 CFU/ml. This meant that the two bacteria solutions were prepared according to the required concentrations.

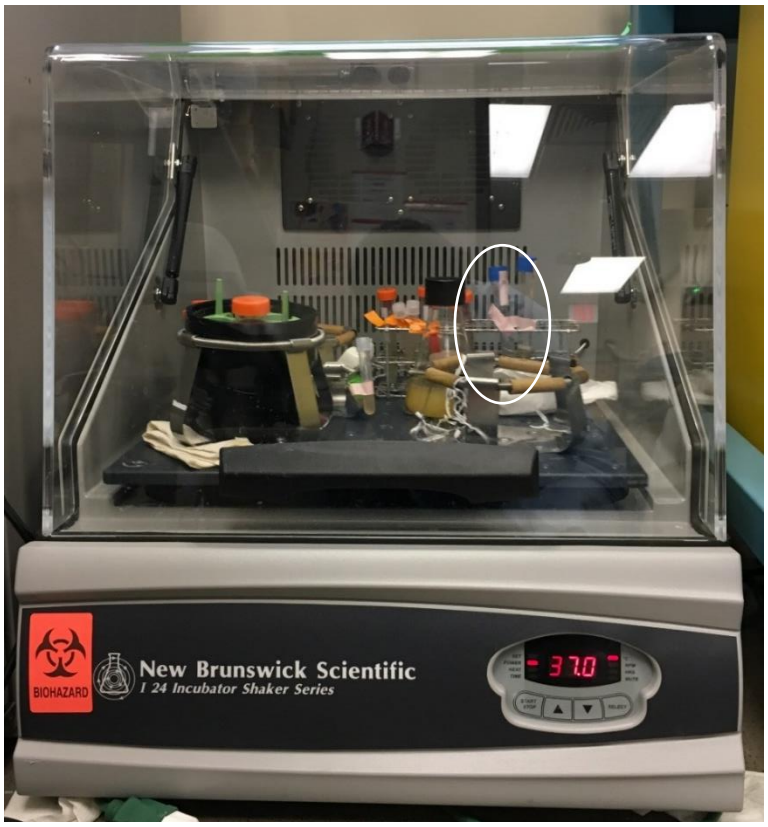

Figure 3.13 Thermostatically controlled incubator shaker.

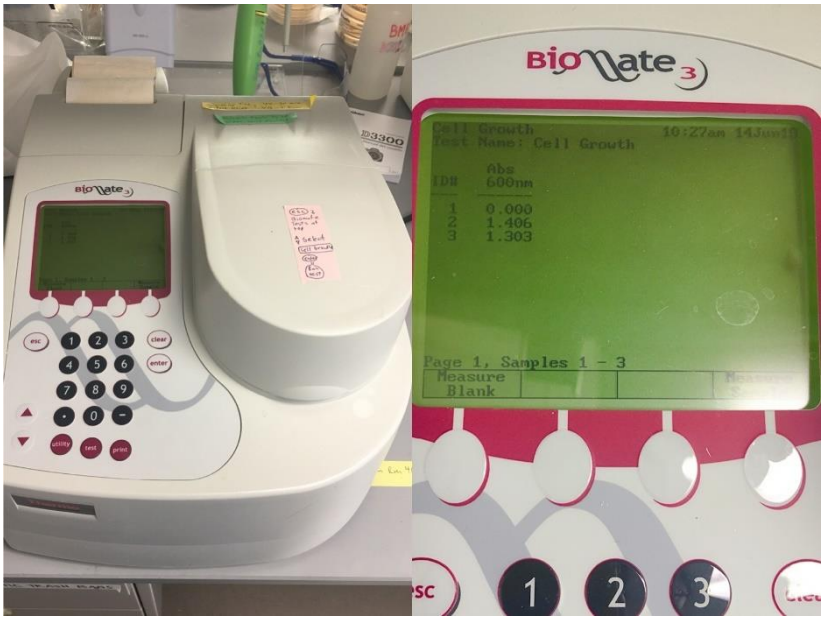

Figure 3.14 Thermo Biomate Spectrometer showing the measurements of optical density at 600nm.

3.3.4.3 Qualitative Antimicrobial Test

According to the paper published in the AATCC Journal (Lamba et al, 2017), a new antimicrobial test method was described which was followed in this study. Clean mesh specimens measuring 8mm square were placed in a 24-well plate in triplicate for each sample group. During pretesting, a high bacterial concentration (10^4 CFUs) was applied and grown on the knitted meshes and no differences were observed between the groups. Then 20µl of the bacterial solutions (30~50 CFUs) were deposited onto the specimens which were agitated to evenly mix the bacterial solution (Figure 3.15). And DI water was added around the wells to maintain the humidity. Then the plates were placed in an incubator at 37 ℃. After a predetermined incubation time of 2h, 6h and 24h, the samples were removed from the 24-well plate (Figure 3.16) and placed on TSA plates. The plates were then incubated at 37 ℃ for 14h, 24h and 48h, and plates were observed and bacterial survival was assessed in terms of growth (G), reduced growth (RG) or no-growth (NG).

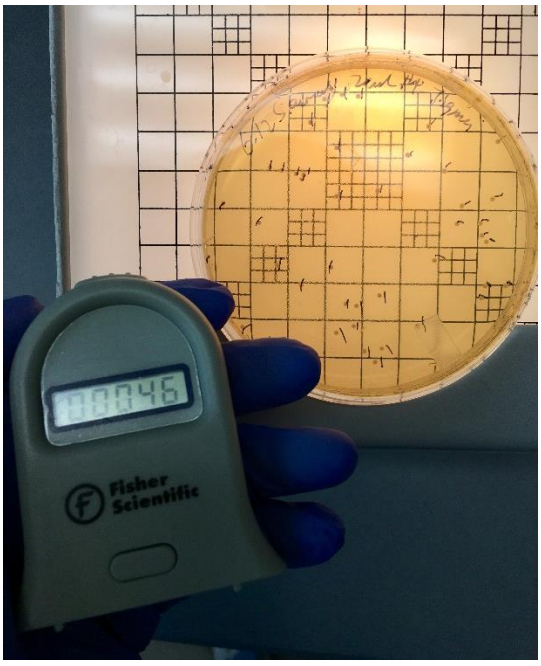

Figure 3.15 Counting bacteria in a 20 µl bacteria solution.

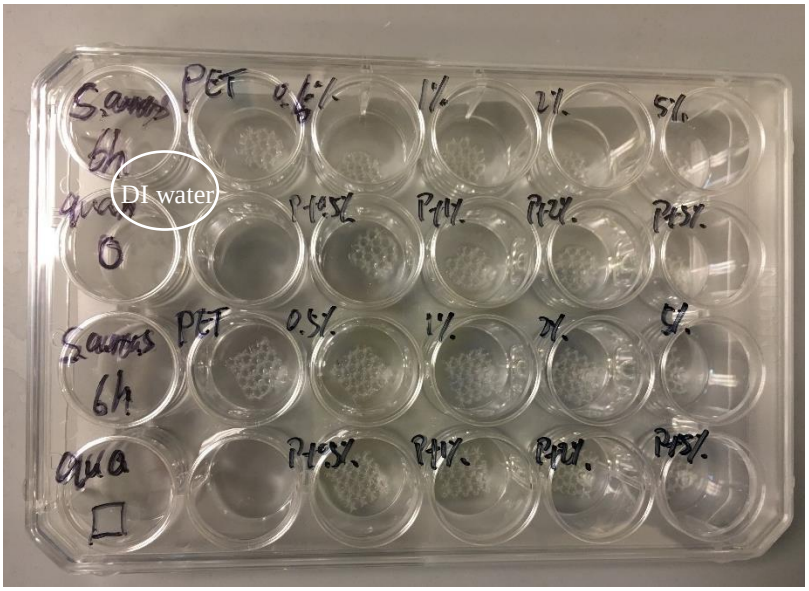

Figure 3.16 The identified square mesh specimens in a 24-well plate.

3.3.4.4 Inhibition Zone Test

According to the previous work describing antimicrobial testing of hernia meshes (Pérez-Köhler, García-Moreno, Bayon, Pascual, & Bellón, 2015), the inhibition zone approach was used. The bacteria solution was prepared with 10^6 CFU/ml. Circular fabric samples, 1cm in diameter, were cut and washed. TSA plates were inoculated with each of the two prepared bacterial solutions by applying and evenly spreading bacteria from a pre-sterilized disposable swab 3 times with 3 directions. Two specimens of each sample were applied to the TSA plates and incubated at 37 ℃ for 14h and 24h. After the respective incubation times the plates were observed and the diameters of the zones of inhibition were measured.

3.4 Statistic Analysis

All values were calculated and reported in terms of the mean and standard deviation. All statistical comparisons were performed using ANOVA analysis and the Tukey post hoc test to compare the means between the different groups. A p-value of 0.05 was assumed to be statistically significant.

CHAPTER 4. RESULTS AND DISCUSSIONS

4.1 Surface Morphology

The scanning electron microscope (SEM) images of the hernia mesh samples are shown in Figure 4.1. The treated and untreated samples are compared and the effect of different concentrations of CMC and plasma treatment are discussed below.

4.1.1 Effect of Plasma Treatment

Plasma treatment was one of the techniques used to modify the surface of the hernia mesh and may have changed the morphology of the fibers. In order to evaluate the effect of the plasma treatment, the untreated control sample and the 5% CMC treated samples are compared to the plasma treated and plasma treated + 5% CMC samples in the following section.

The warp knitted structure is shown in Figs. 4.1 (a) (c). Both the untreated control sample and the plasma treated sample have a smooth surface appearance at low magnification. But there are some wrinkles around the bent fibers in Figs.4.1 (b) (d). Some particles are visible under higher magnification (Figure 4.1 and Figure 4.2) and the size of those irregular shaped particles is around 0.8~1.5 μm (Figure 4.3). These small particles could be some impurities in the air that were absorbed onto the polymer surface during storage, or the extrusion or other production process. Additionally, there appeared to be no etching of the surface during plasma treatment, no matter the level of CMC crosslinking. So, the plasma treatment didn't change the morphology of the fibers'

surface and elemental analysis was needed to clarify whether or not there was a difference in composition.

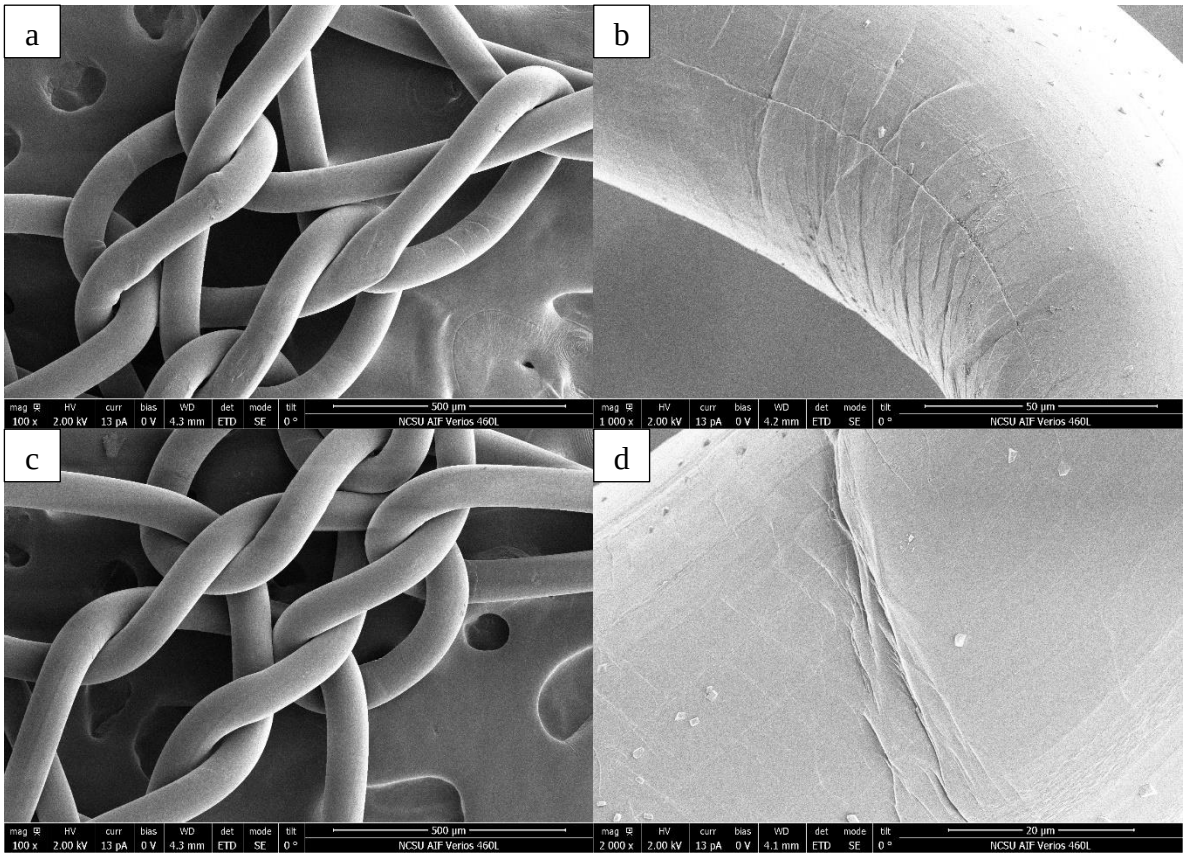

Figure 4.1 SEM photomicrographs of hernia mesh
(a) Untreated control sample (magnification 100×),
(b) Untreated control sample (magnification 1000×),
(c) Plasma treated sample (magnification 100×),
(d) Plasma treated sample (magnification 2000×).

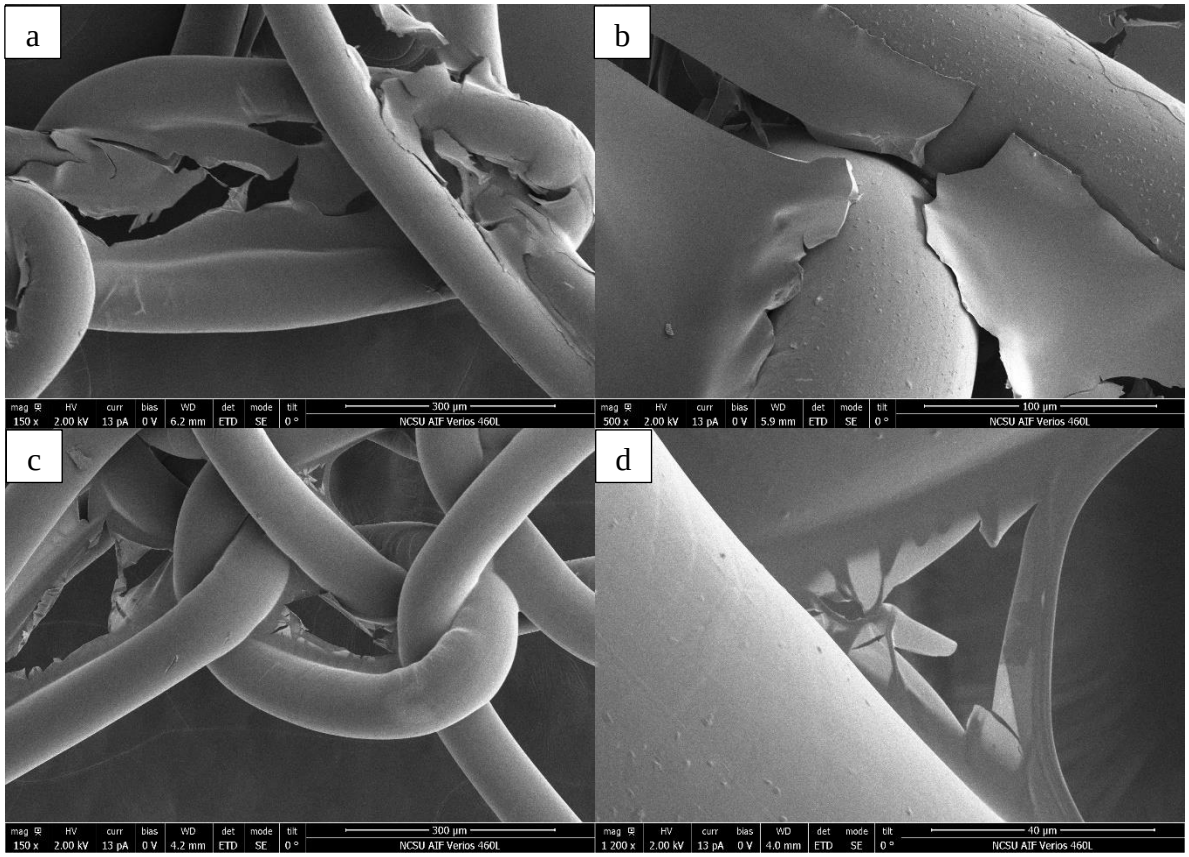

Figure 4.2 SEM photomicrographs of the hernia mesh
(a) Control sample treated with 5% CMC (magnification 150×),
(b) Control sample treated with 5% CMC (magnification 500×),
(c) Sample treated with plasma + 5% CMC (magnification 150×),
(d) Sample treated with plasma + 5% CMC (magnification 1200×).

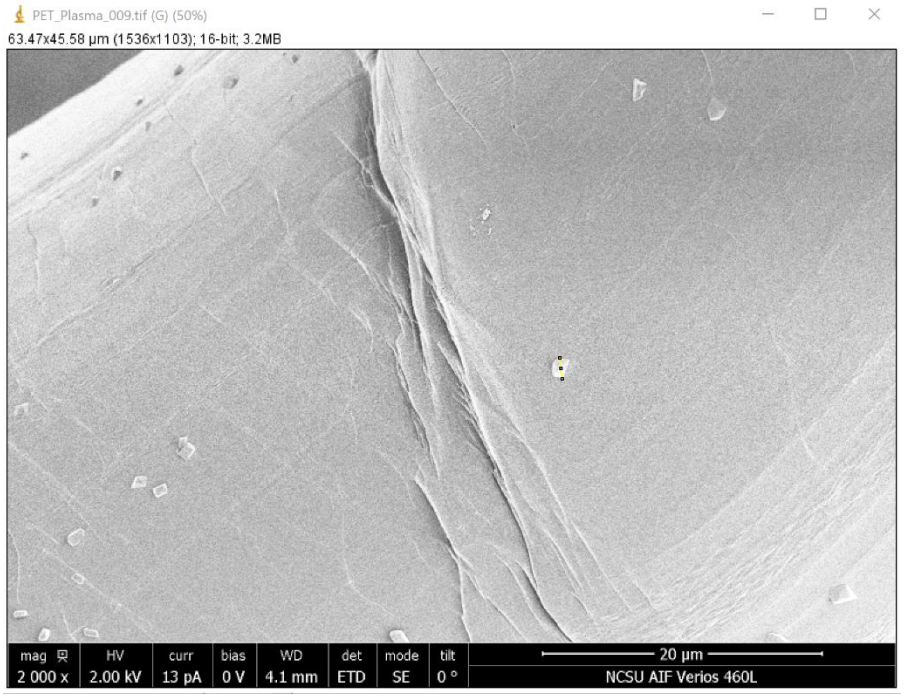

Figure 4.3 SEM photomicrograph of hernia mesh plasma treated sample showing presence of surface particles (magnification 2000×).

4.1.2 Effect of Varying the CMC Concentration

The amount of carboxymethyl chitosan (CMC) applied during the plasma treatment was varied from 0.5% to 5% in a series of 4 samples. The thickness of the resulting cross-linked thin films on the surface of the mesh were observed and measured by SEM. The five different groups for analysis were 1) the untreated control sample, 2) the plasma treated samples with 0.5% CMC, 3) the plasma treated samples with 1% CMC, 4) the plasma treated sample with 2% CMC and 5) the plasma treated samples with 5% CMC.

Figure 4.4 SEM photomicrographs of the hernia mesh showing
(a) Untreated control sample (magnification 100×),
(b) Untreated control sample (magnification 1000×),
(c) Plasma treated sample with 0.5% CMC (magnification 200×),
(d) Plasma treated sample with 0.5% CMC (magnification 1500×),
(e) Plasma treated sample with 1% CMC (magnification 150×),
(f) Plasma treated sample with 1% CMC (magnification 350×),
(g) Plasma treated sample with 2% CMC (magnification 80×),
(h) Plasma treated sample with 2% CMC (magnification 1500×),
(i) Plasma treated sample with 5% CMC (magnification 150×),
(j) Plasma treated sample with 5% CMC (magnification 1200×).

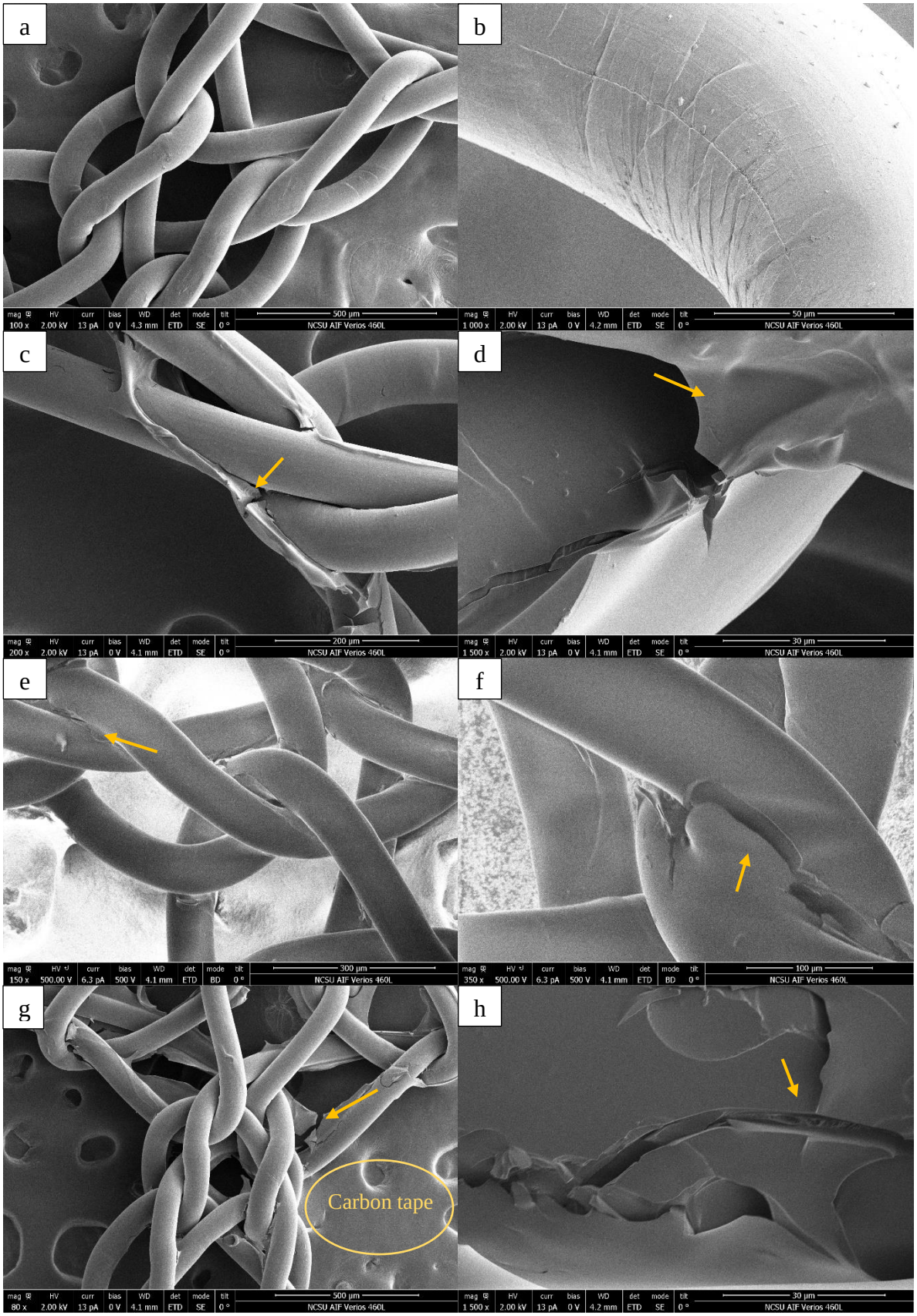
a
b
c
d
e
f
g
h
Carbon tape
NCSU AIF Verios 460L

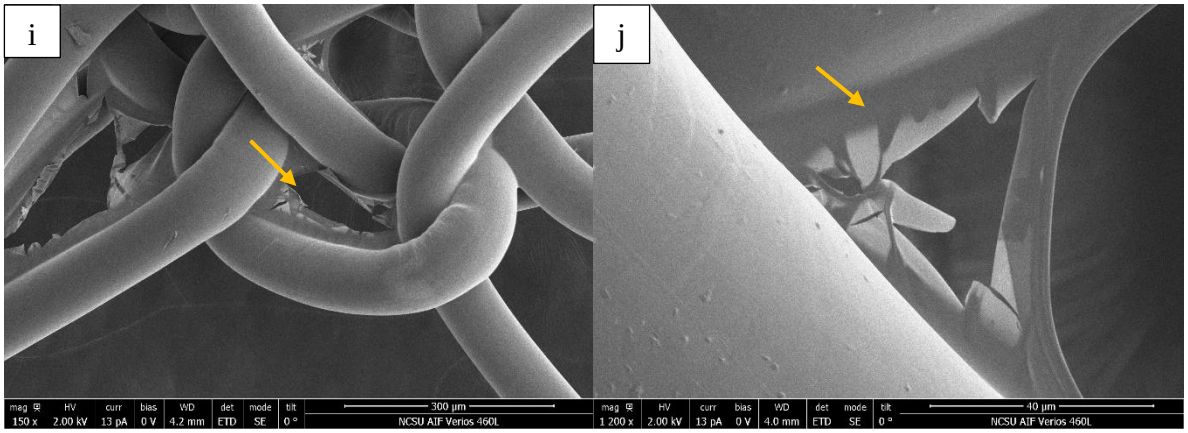

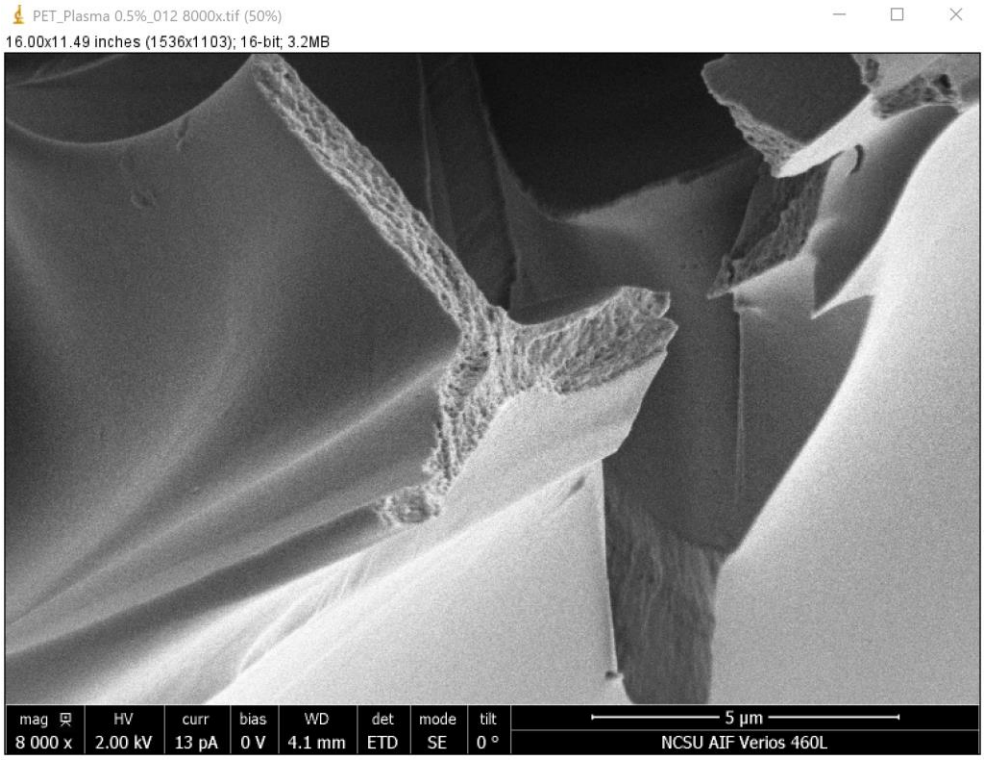

Figure 4.5 SEM photomicrograph of hernia mesh following plasma treatment and used for thickness measurements.

It was easy to view the layer at the places where the fibers crossed (Figure 4.4). And some cracks and fractures were observed at the crossings and contact places between fibers. On account of the viscosity of the higher concentration CMC/CA solutions the treated meshes were sticky, and after oven drying and crosslinking, the mesh samples stuck to the foil, and the fractures may have been

created when samples were removed from the aluminum foil. The chitosan (CMC) layer present around the fibers was thin and varied in thickness between 0.6~1.7 μm measured from the exposed crack areas (Figure 4.5). It was assumed that the thickness measurement at the defect or cracks was the same thickness as in the smooth undamaged areas. There were no apparent differences between the five sample groups in terms of the CMC film morphology. The 1% CMC group without a gold-palladium coating was not as clearly visible as the other groups (Figure 4.4 e & f). While the specimens could still be viewed by FESEM without a conductive coating, the results without coating were not as clear.

4.2 Chemical Analysis

After plasma and CMC treatment, the functional groups on the surface were modified, and various analytical methods were used to detect the chemical changes at the surface of the fibers.

4.2.1 Fourier Transform Infrared (FTIR) Spectroscopy

In general, atmospheric plasma uses an unreactive gas, such as helium, to create a stable discharge environment. The addition of a reactive gas, such as oxygen, can then generate active groups on the surface that can participate in subsequent reactions. One type of reaction might have involved the bonding of the CMC to the polyester macromolecular chains by reacting atomic oxygen, oxygen molecules and superoxide free radicals with the unsaturated bonds on the surface of the polyester. For FTIR analysis, four groups of samples were tested: 1) the untreated control, 2) the plasma treated sample, 3) the 1% CMC treated sample and 4) the plasma treated and 1% CMC treated sample.

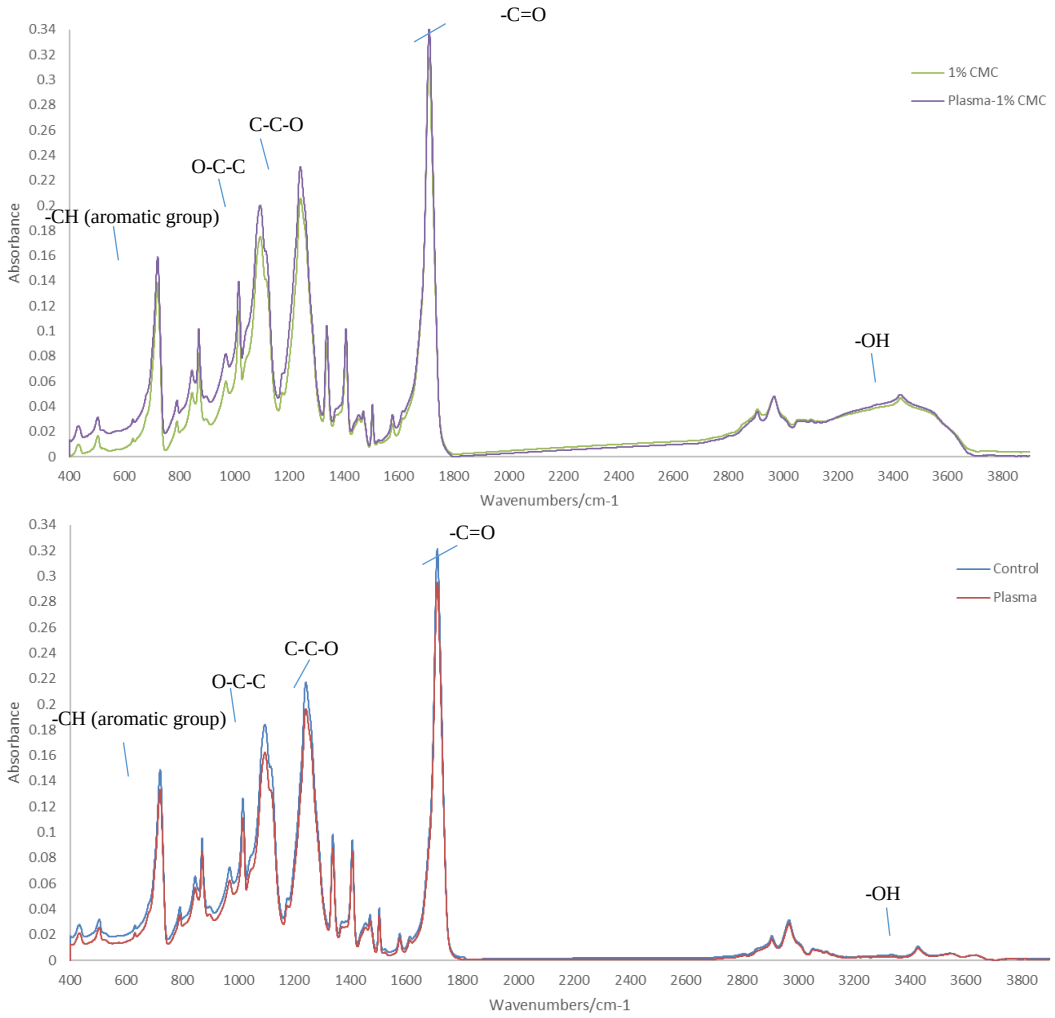

Figure 4.6 FTIR spectra (Above) of the 1% CMC treated samples with and without plasma exposure and (Below) of the untreated control samples with and without plasma exposure.

The plasma treatment was operated under atmospheric pressure. In Figure 4.6, the four major peaks associated with the inherent structure of the PET were the terephthalic acid ester C=O group at 1711 cm^{-1}, the asymmetric C-C-O and the O-C-C stretching at 1243 and 1095 cm^{-1}, respectively, and the C-H wagging vibrations from the aromatic structure at 721 cm^{-1} (Strain et al., 2015). The spectrum of the control sample is similar to that of the plasma treated sample, and the curve for the 1% CMC treated sample is similar to that for the plasma sample treated with 1% CMC. So

using FTIR, there were no apparent new peaks corresponding to the presence of new functional groups between the plasma treated and other samples.

For the chemical structure of CMC, generally the C-N stretch bands of chitosan are visible on spectra around 1350–1250 and 1180–1040 cm^{-1}. Then the broad band above 3100 cm^{-1} corresponds to the -OH which belongs to the (CO)O-H structure (Aubert-Viard et al., 2015). The N-H vibration band (1560 cm^{-1}) belongs to the amino groups (Yadav & Shivakumar, 2012).

Due to the existence of the PET aromatic ester C=O stretching vibration in the 1550-1850 cm^{-1} domain, it was not possible to find evidence of a CMC -N-H vibration around 1560 cm^{-1}. And C-N stretching bands of chitosan are around 1350–1250 and 1180–1040 cm^{-1} which is also the domain of the asymmetric C-C-O and the O-C-C stretching at 1243 and 1095 cm^{-1} for PET. So in Figure 4.6, the characteristic peaks of CMC were covered by the PET absorptions. This means that FTIR was unable to identify any new groups that would demonstrate the presence of cross-linked carboxymethyl chitosan.

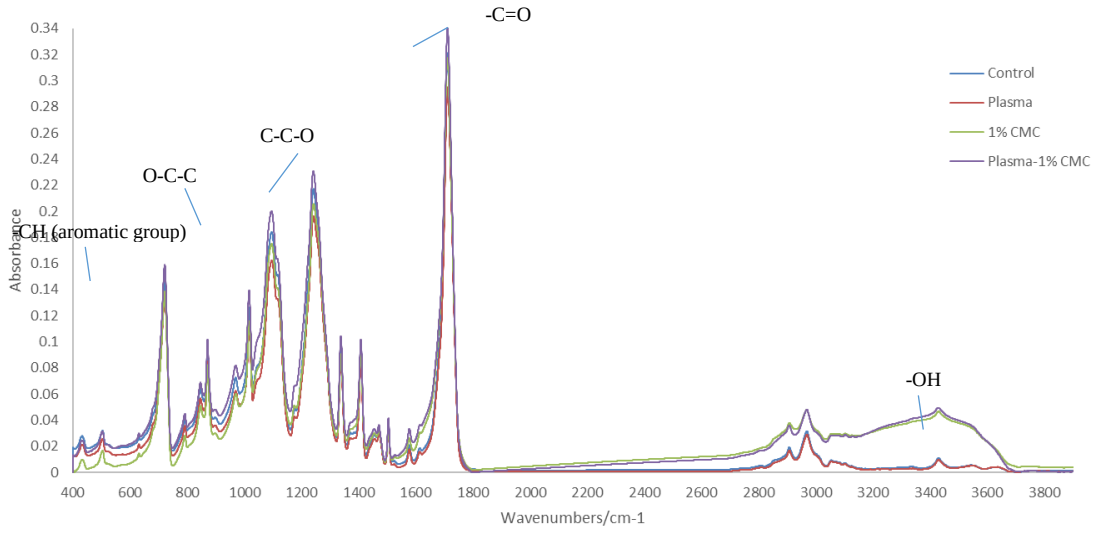

Figure 4.7 FTIR spectra of the untreated control sample, the plasma treated sample, the 1% CMC treated and the plasma treated + 1% CMC sample.

Table 4.1 FTIR absorbance values and calculated ratios of OH/CH.

	Control	1% CMC	Plasma	Plasma+1% CMC
-OH(3429cm-1)	0.011	0.046	0.010	0.050
-CH(721cm-1)	0.149	0.138	0.133	0.159
Ratio of OH/CH	0.072	0.336	0.072	0.311

If the material is not modified, then the chemical composition and the ratio of the functional groups will remain the same. But at the same time, the ratio of OH / CH will increase significantly, particularly after 1% CMC treatment. The CH aromatic group only exists in PET, while the OH group exists in both CMC and PET. So the ratio of OH / CH rose from 0.072 to 0.336 after 1% CMC treatment, and the ratio for the plasma group also rose from 0.072 to 0.311, which means that the surface was coated with O-CMC linkages and citric acid containing OH groups.

4.2.2 X-Ray Photoelectron Spectroscopy (XPS)

PET is a high molecular weight polymer composed of carbon (C), oxygen (O) and hydrogen (H). After the plasma treatment, the oxygen elemental composition increased from 30% to 36% (Table 4.2) whereas the composition of 5% CMC treated sample with no plasma treatment did not change significantly. This means the He/O_2 (99%/1%) carrier gas activated the surface of the PET mesh successfully with the addition of functional groups such as -COOH and -OH and active species such as singlet oxygen, $O\cdot$, during the plasma treatment.

Figure 4.8 X-ray photoelectron spectroscopy (XPS) spectra for the hernia mesh samples: (a) Untreated control sample, (b) Plasma treated sample, (c) Plasma treated + 0.5% CMC exposed sample, (d) Plasma treated + 1% CMC exposed sample, (e) Plasma treated + 2% CMC exposed sample, (f) Plasma treated + 5% CMC exposed sample, (g) 5% CMC exposed reference sample.

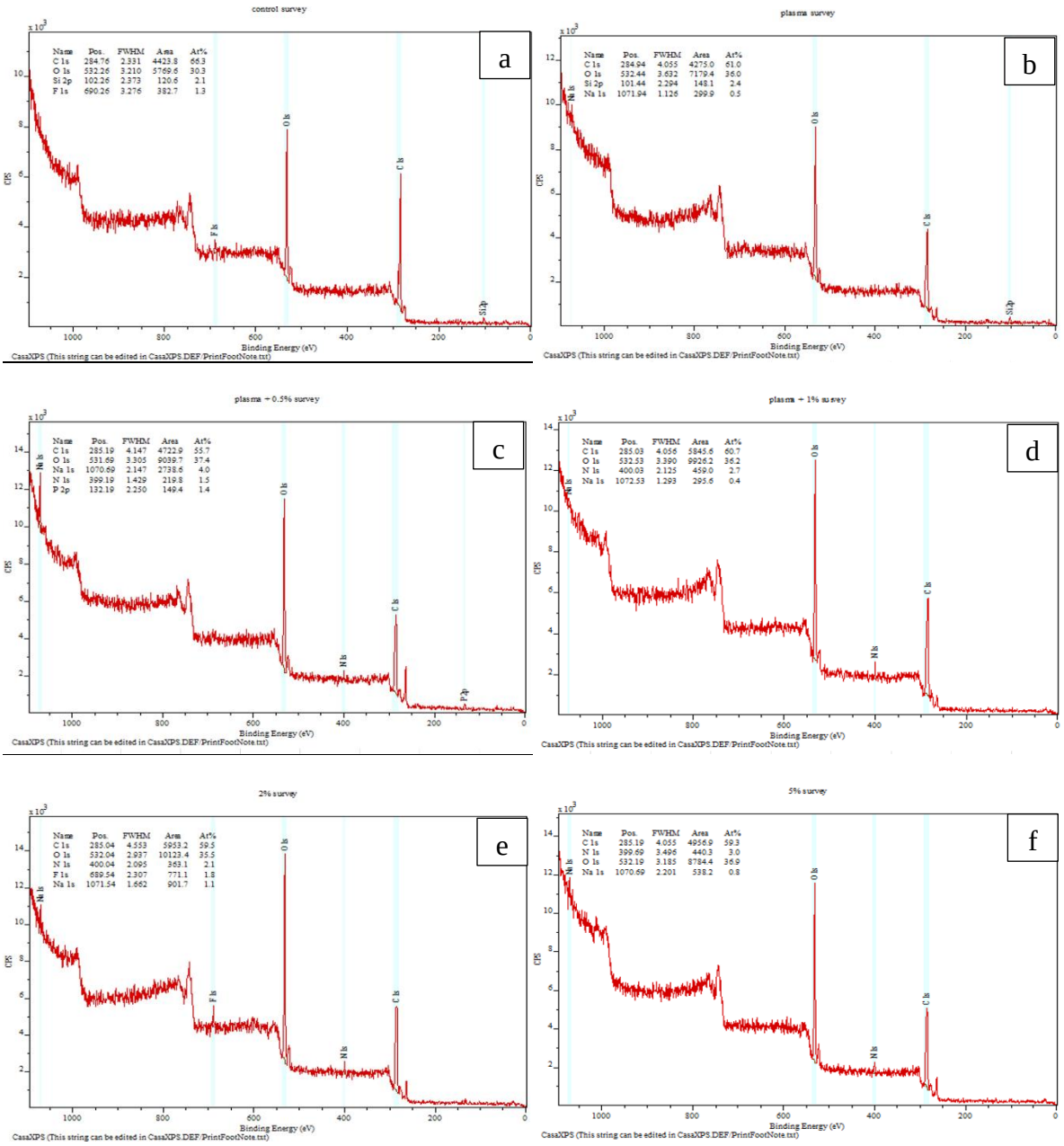
control survey
a
Name Pos. FWHM Area At%
C 1s 284.76 2.831 4423.8 65.3
O 1s 532.26 3.210 5769.6 30.3
Si 2p 102.26 2.373 120.6 2.1
F 1s 690.26 3.276 382.7 1.3
O 1s
C 1s
F 1s
Si2p
CPS
Binding Energy (eV)
CasaXPS (This string can be edited in CasaXPS.DEF/PrintFootNote.txt)
plasma survey
b
Name Pos. FWHM Area At%
C 1s 284.94 4.055 4275.0 51.0
O 1s 532.44 3.632 7179.4 36.0
Si 2p 101.44 2.294 148.1 2.4
Na 1s 1071.94 1.126 299.9 0.5
Na 1s
O 1s
C 1s
Si2p
CPS
Binding Energy (eV)
CasaXPS (This string can be edited in CasaXPS.DEF/PrintFootNote.txt)
plasma + 0.5% survey
c
Name Pos. FWHM Area At%
C 1s 285.19 4.147 4722.9 55.7
O 1s 531.69 3.305 9039.7 37.4
Na 1s 1070.69 2.147 2738.6 4.0
N 1s 399.19 1.429 219.8 1.5
P 2p 132.19 2.250 149.4 1.4
Na 1s
O 1s
C 1s
N 1s
P 2p
CPS
Binding Energy (eV)
CasaXPS (This string can be edited in CasaXPS.DEF/PrintFootNote.txt)
plasma + 1% survey
d
Name Pos. FWHM Area At%
C 1s 285.03 4.056 5845.6 60.7
O 1s 532.53 3.390 9926.2 36.2
N 1s 400.03 2.125 459.0 2.7
Na 1s 1072.53 1.293 295.6 0.4
Na 1s
O 1s
C 1s
N 1s
CPS
Binding Energy (eV)
CasaXPS (This string can be edited in CasaXPS.DEF/PrintFootNote.txt)
2% survey
e
Name Pos. FWHM Area At%
C 1s 285.04 4.553 5953.2 59.5
O 1s 532.04 2.937 10123.4 35.5
N 1s 400.04 2.095 363.1 2.1
F 1s 689.54 2.307 771.1 1.8
Na 1s 1071.54 1.662 901.7 1.1
Na 1s
O 1s
F 1s
C 1s
N 1s
CPS
Binding Energy (eV)
CasaXPS (This string can be edited in CasaXPS.DEF/PrintFootNote.txt)
5% survey
f
Name Pos. FWHM Area At%
C 1s 285.19 4.055 4956.9 59.3
N 1s 399.69 3.496 440.3 3.0
O 1s 532.19 3.185 8784.4 36.9
Na 1s 1070.69 2.201 538.2 0.8
Na 1s
O 1s
C 1s
N 1s
CPS
Binding Energy (eV)
CasaXPS (This string can be edited in CasaXPS.DEF/PrintFootNote.txt)

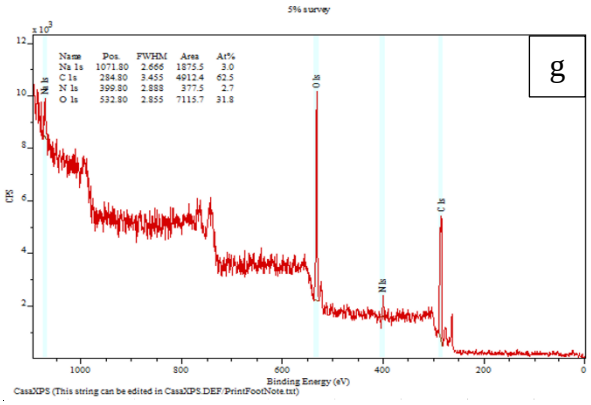

Table 4.2 Elemental analytical results after each treatment.

Sample	C (%)	O (%)	N (%)	Na (%)	F (%)	Si (%)	P (%)
Control	66.30%	30.30%			1.30%	2.10%	/
Plasma	61.00%	36.00%		0.50%	/	2.40%	/
Plasma+0.5% CMC	55.70%	37.40%	1.50%	4.00%	/	/	1.40%
Plasma+1% CMC	60.70%	36.20%	2.70%	0.40%	/	/	/
Plasma+2% CMC	59.50%	35.50%	2.10%	1.10%	1.80%	/	/
Plasma+5% CMC	59.30%	36.90%	3.00%	0.80%	/	/	/
5% CMC	62.50%	31.80%	2.70%	3.00%	/	/	/

The major difference in elemental analysis between PET and the CMC treated samples is the presence of nitrogen in the CMC treated samples. In Table 4.2, the nitrogen elemental composition of all the CMC groups increased significantly, but not in a linear fashion. The nitrogen composition increased significantly from 0.5% CMC to 1% CMC, but between the 2% and the 5% CMC treated samples there was no significant change in nitrogen composition. Thus, the extent of CMC addition to the surface appears to increase up until the 1% CMC concentration but not beyond. Furthermore, there was no difference in nitrogen content between the plasma treatment + 5% CMC and the 5% CMC group with no plasma treatment. This means that the plasma treatment did not change the efficiency of the CMC surface treatment.

Given that the antimicrobial activity of the CMC molecule depends on a protonated amine group, the maximum amine concentration was calculated for each of the CMC treated samples. It was found that the maximum potential amine concentration was only 3.4% which inevitably limited the level of antimicrobial activity of the CMC samples. As a result of CA crosslinking, the actual amine group concentration would have been significantly lower than 3.4%.

4.3 Mechanical Property

4.3.1 Probe Bursting Test

The bursting strength test measures the mechanical performance of a knitted textile structure by applying a probe at right angles to the plane of the fabric. Therefore, the force applied to the testing area is uniform in all directions. Three groups of samples were tested: the untreated control, the 5% CMC coated sample and the plasma treated + 5% CMC coated sample. The experimental results for the three different hernia mesh samples are presented in terms of their maximum bursting stress (Formula calculation) in Figure 4.9 and their extension at peak load in Figure 4.10.

In Figure 4.9, the bursting stress of the plasma treated plus 5% CMC coated, and the 5% CMC coated without plasma samples decreased from 0.90 to 0.78 and to 0.71 respectively. The bursting stress values for both the CMC coated and the plasma treated samples were significantly lower than the untreated control mesh ($p \leq 0.05$). This means that both the CMC coating and the plasma treatment were found to significantly reduce the bursting strength of the PET warp knitted hernia mesh. Moreover, the standard deviation of both the CMC coated and the plasma treated samples increased from 0.05 to 0.08 and to 0.10, which means that both the coating and the plasma

treatment contribute to increasing the variability in the mechanical performance of the knitted mesh structures.

In Figure 4.10, the extension at peak load of CMC and plasma groups decreased from 8.09 to 6.37 and to 7.25. Similar to the bursting stress measurements, the extension at peak load for both the CMC coated and the plasma treated samples were significantly lower than the untreated control mesh ($p \leq 0.05$). This means that both the CMC coating and the plasma treatment made the mechanical properties significantly more brittle. An explanation for this change is likely due to the surface treatment and/or the high temperature crosslinking process. Also, the standard deviation of both the CMC coated and plasma treated samples increased from 0.22 to 0.31 and to 0.55, which means that both the coating and the plasma treatment increased the variability of the mesh's mechanical performance.

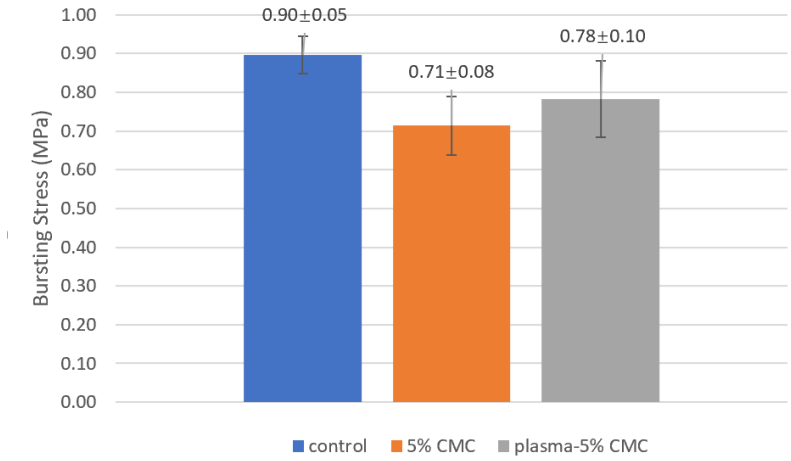

Figure 4.9 Bursting stress for the three mesh samples.

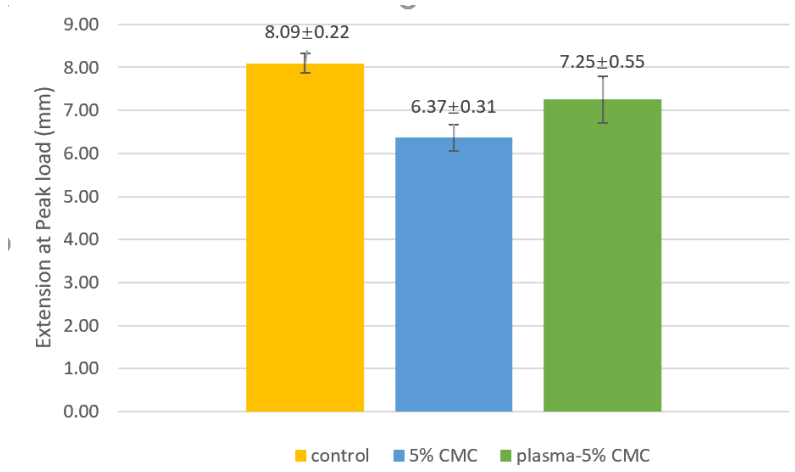

Figure 4.10 Extension at peak load for the three mesh samples.

4.4 Antimicrobial Test

4.4.1 Qualitative Antimicrobial Test

Based on the Lamba et al's published paper in the AATCC Journal (Lamba et al., 2017) there are three levels of antimicrobial performance: namely, growth (G), reduced growth (RG) and no growth (NG). For some bacteria on some substrates, the specific area of bacterial growth is difficult to determine. So in order to determine whether or not their *E. coli* bacterial count is reduced, their areas were counted and compared (Figure 4.11 and Table 4.3). The micro-organism, *S. aureus*, grew more slowly than *E. coli*, so for some groups they didn't form a measurable area. In this case, the bacteria grew on the mesh fibers where they were visible, so they were reported in terms of G, RG or NG (Figure 4.12).

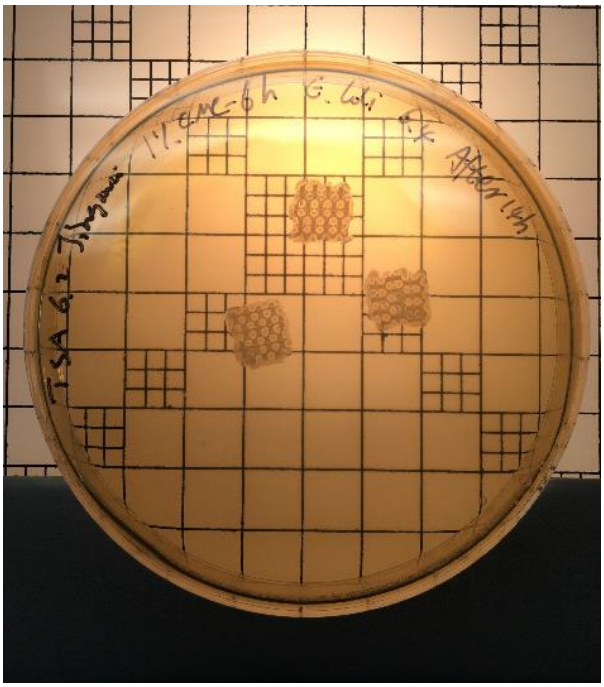

Figure 4.11 Visible bacteria area of *E. coli* after 14 hours of incubation.

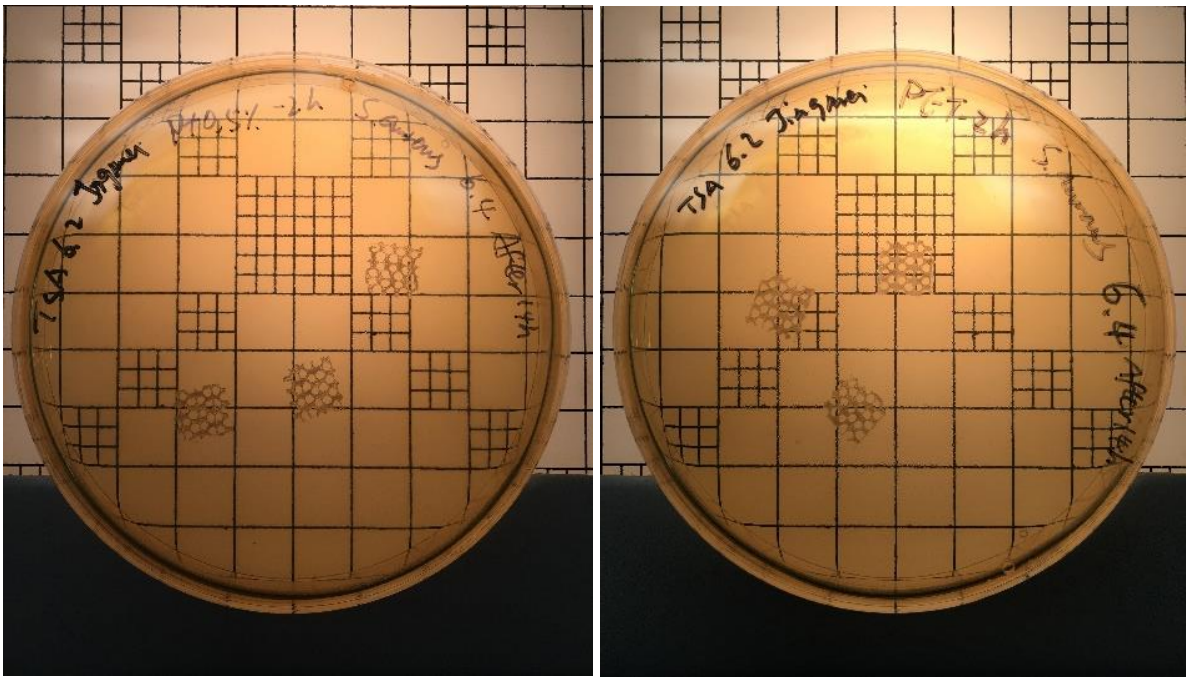

Figure 4.12 Visible colonies of *S. aureus* after 14 hours of incubation.

In Table 4.3, the areas of bacterial growth are reported after 2h, 6h and 24h of contact time and after being transferred from the 24-well plate to the TSA plate for incubation. *E. coli* grew more rapidly than *S. aureus*, so that after 14h of incubation, the bacterial growth area was found to be larger with longer incubation times. When counting the area of growth, the small square was $1cm^2$, and the measurement of the bacteria area was based on this area. Each average value was calculated from three specimens. For all the *E. coli* results, the areas for the CMC coated sample and the plasma treated sample were similar to the control group after the same contact and incubation times (Table 4.4 and Table 4.5). This means that the CMC coating did not provide any antimicrobial activity. So all the groups are reported as "G".

Some areas in the 6h group were marginally smaller than in the 2h group. However, please note that the bacterial solution concentration was around 30~50 CFU/20 μL, and all samples for the same contact time used the same solution. So this is a case of experimental error. While growth areas for the 24h contact time sample were significantly larger than for the 2h contact time sample, this points to the fact that the bacteria were growing continuously. So, for the CMC coated and the plasma samples, longer contact times led to larger areas of bacterial growth. This also demonstrates that the CMC used in this experiment did not have antimicrobial activity.

Table 4.3 Areas of growth (cm^2) for *E. coli* after different periods of contact and 14h of incubation.

After 14h of incubation	E. Coli-2h	E. Coli-6h	E. Coli-24h
control	0.98	0.95	1.74
0.5% CMC	1.02	1.05	1.47
plasma+0.5% CMC	0.92	0.88	1.13
1% CMC	1.13	1.00	1.71
plasma+1% CMC	1.08	1.24	1.32
2% CMC	1.11	1.02	1.55
plasma+2% CMC	1.21	0.83	1.29
5% CMC	1.21	1.34	1.50
plasma+5% CMC	1.36	1.04	1.17

Table 4.4 Areas of growth (cm^2) for *E. coli* after different periods of contact and 24h of incubation.

After 24h of incubation	E. Coli-2h	E. Coli-6h	E. Coli-24h
control	1.58	1.14	1.84
0.5% CMC	1.68	1.19	1.63
plasma+0.5% CMC	1.69	1.19	1.47
1% CMC	2.05	1.21	1.79
plasma+1% CMC	1.46	1.56	1.74
2% CMC	1.75	1.25	1.71
plasma+2% CMC	1.67	1.48	1.53
5% CMC	1.98	1.55	1.54
plasma+5% CMC	1.81	1.43	1.31

Table 4.5 Areas of growth (cm^2) for *E. coli* after different periods of contact and 48h of incubation.

After 48h of incubation	E. Coli-2h	E. Coli-6h	E. Coli-24h
control	1.96	1.78	2.79
0.5% CMC	2.01	1.84	2.50
plasma+0.5% CMC	2.30	1.71	2.28
1% CMC	2.14	1.87	2.75
plasma+1% CMC	2.22	2.04	2.39
2% CMC	2.26	1.88	2.64
plasma+2% CMC	2.10	2.08	2.57
5% CMC	2.10	1.99	2.54
plasma+5% CMC	2.25	2.15	2.61

The results in Table 4.6 show that *S. aureus* grew slower on the mesh samples and no growth area of bacteria was formed after 14h and 24h of culture in the incubator. But according to observation of the visible colonies, they all grew at a similar rate and so were all marked as G (Table 4.6 and Table 4.7). After 48h of incubation, the growth areas for *S. aureus* were countable (Table 4.8) and the growth areas of all nine samples were similar for the same contact time of 2h, 6h or 24h. In other words, longer contact times, led to larger areas of bacterial growth. So, regardless of the contact time, *S. aureus* continued to grow on all samples. This means that the CMC coating did not inhibit the growth of the bacteria.

Table 4.6 Areas of growth (cm^2) for *S. aureus* after different periods of contact and 14h of incubation.

After 14h of incubation	S. Aureus-2h	S. Aureus-6h	S. Aureus-24h
control	G	G	G
0.5% CMC	G	G	G
plasma+0.5% CMC	G	G	G
1% CMC	G	G	G
plasma+1% CMC	G	G	G
2% CMC	G	G	G
plasma+2% CMC	G	G	G
5% CMC	G	G	G
plasma+5% CMC	G	G	G

Table 4.7 Areas of growth (cm^2) for *S. aureus* after different periods of contact and 24h of incubation.

After 24h of incubation	S. Aureus-2h	S. Aureus-6h	S. Aureus-24h
control	G	G	G
0.5% CMC	G	G	G
plasma+0.5% CMC	G	G	G
1% CMC	G	G	G
plasma+1% CMC	G	G	G
2% CMC	G	G	G
plasma+2% CMC	G	G	G
5% CMC	G	G	G
plasma+5% CMC	G	G	G

Table 4.8 Areas of growth (cm^2) for *S. aureus* after different periods of contact and 48h of incubation.

After 48h of incubation	S. Aureus-2h	S. Aureus-6h	S. Aureus-24h
control	0.99	1.12	1.25
0.5% CMC	1.08	1.23	1.31
plasma+0.5% CMC	1.03	1.09	1.15
1% CMC	1.05	1.05	1.06
plasma+1% CMC	1.02	1.18	1.21
2% CMC	1.03	1.03	1.04
plasma+2% CMC	1.08	1.10	1.18
5% CMC	0.96	1.04	1.03
plasma+5% CMC	0.89	0.93	1.02

4.4.2 Inhibition Zone

After 14h and 24h of incubation, the samples were observed microscopically. No inhibition zone was observed on the plate for any of the nine groups, and no differences were observed between the untreated control sample and the CMC coated or the plasma treated samples. In Figure 4.13 and 4.14, neither the untreated control, nor the 5% CMC coated sample following plasma treatment samples showed an inhibition zone. CMC is water soluable, but after crosslinking CMC will not dissolve in aqueous media. So the negative inhibition zone result could be caused by either a diffusion problem or poor antimicrobial activity or both.

Table 4.9 Results for zones of inhibition for *E. coli* and *S. aureus* after different incubation times.

	Inhibition Zone			
	E. Coli-14h	E. Coli-24h	S. Aureus-14h	S. Aureus-24h
control	N	N	N	N
0.5% CMC	N	N	N	N
plasma-0.5% CMC	N	N	N	N
1% CMC	N	N	N	N
plasma-1% CMC	N	N	N	N
2% CMC	N	N	N	N
plasma-2% CMC	N	N	N	N
5% CMC	N	N	N	N
plasma-5% CMC	N	N	N	N

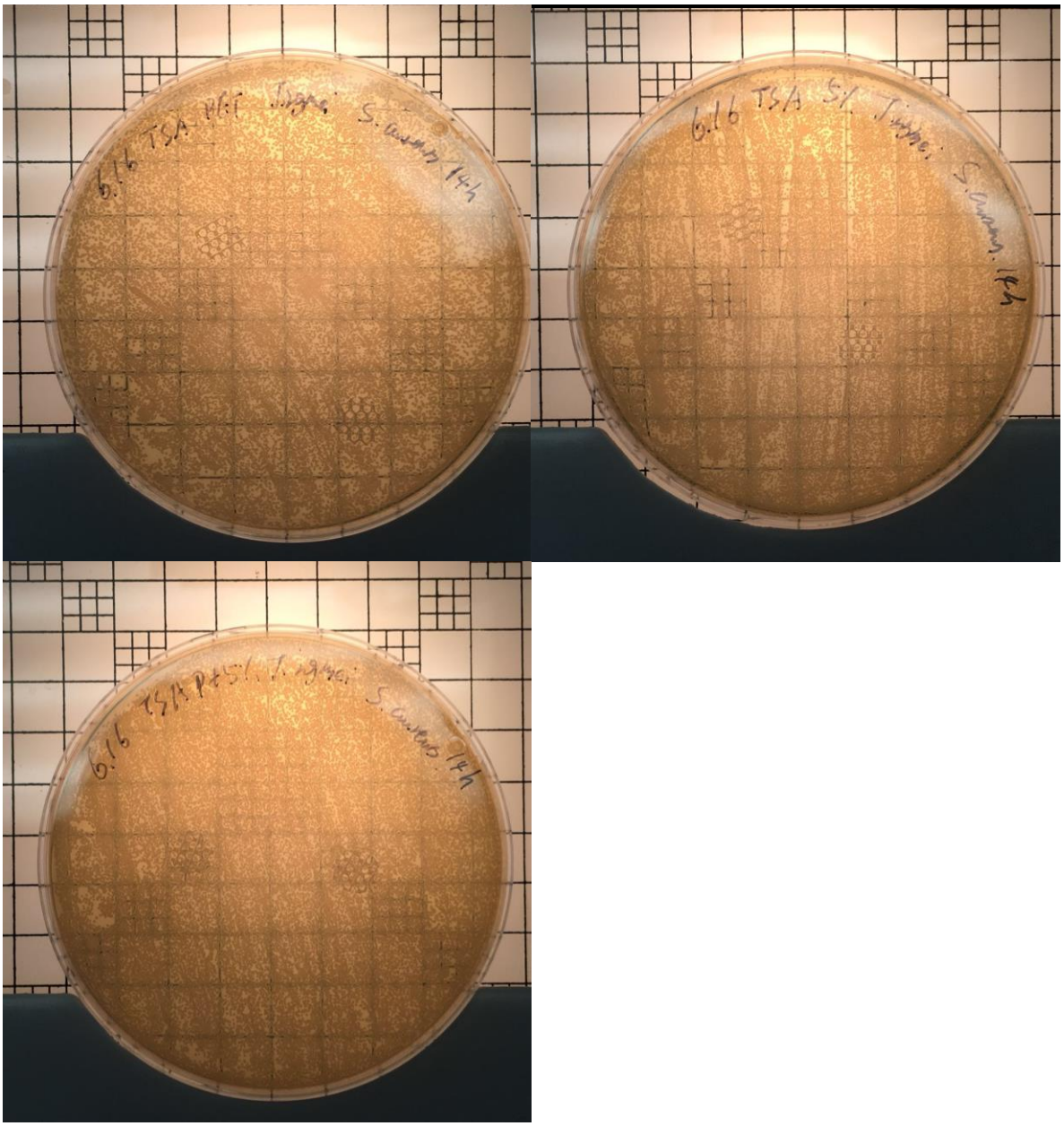

Figure 4.13 Untreated control, 5% CMC coated and plasma treated + 5% CMC samples after 14h incubation with *S. aureus.*

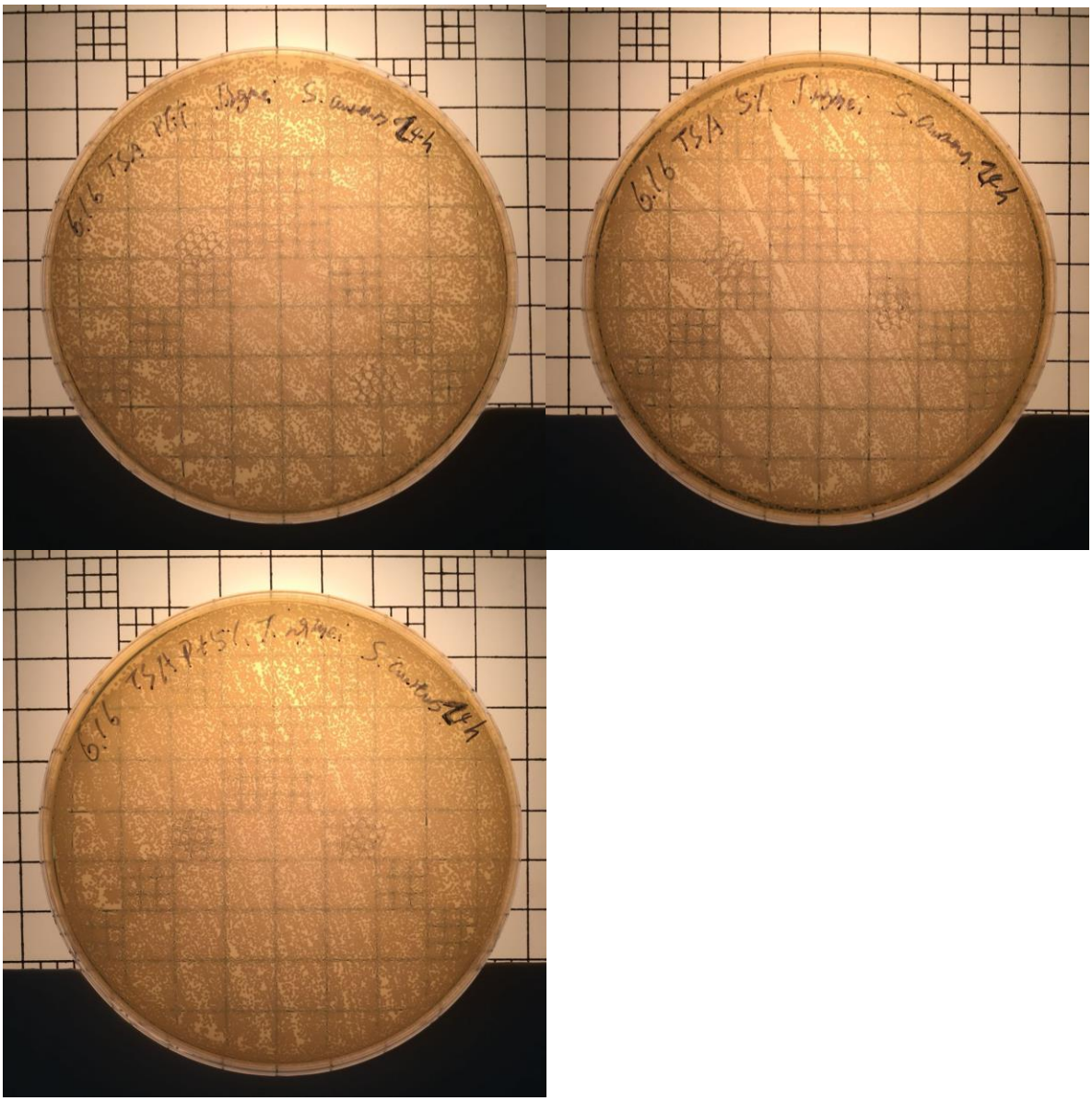

Figure 4.14 Untreated control, 5% CMC coated and plasma treated + 5% CMC samples after 24h incubation with *S. aureus.*

CHAPTER 5. CONLUSIONS AND FUTURE WORK

5.1 Conclusions

By revisiting the six objectives of this study, it is possible to draw specific conclusions for each objective, and to comment on whether or not the objective has been met. If the objective has not been met, then a possible explanation of the reasons is given, which can lead to recommendations for future work and additional studies.

1) The project was successful in applying a carboxymethyl chitosan (CMC) bound crosslinked chemical coating to the surface of a knitted polyester hernia mesh fabric as confirmed by the initial significant increase in –OH functional groups. However, beyond a certain CMC concentration, the chemical grafting did not continue to increase in a steady linear fashion.
2) The application of CMC and cross-linking agent, citric acid (CA), produced thin films on the surface of the PET fibers measuring 0.6~1.7μm in thickness. The concentration of the CMC solution did not change the film thickness or apparent film morphology. Some cracks and fractures of the film were caused by the process of removing the samples from the aluminum foil substrate.
3) The He/O_2 radio frequency plasma did not appear to change the surface morphology of the PET fibers and failed to enhance the CMC non-bound crosslinked physical coating treatment efficiency. While the 99%/1% He/O_2 plasma increased the oxygen content of the PET fiber surface, the additional oxygen content was introduced via functional groups, such as –OH, -COOH and singlet oxygen.
4) FTIR spectroscopy was expected to enable the monitoring of the chemical cross-linking efficiency. However, the characteristic infrared absorption peaks of CMC were covered by the

PET absorptions, which means that FTIR was unable to identify any new groups that would confirm the presence of cross-linked CMC.

5) Both the non-bound crosslinked physical CMC coating of the polyester fibers and the plasma treated chemically grafted and cross-linked CMC treatment reduced the bursting strength of the knitted PET mesh. In particular, the plasma treated chemical treatment affected the bursting strength of the PET mesh more severely than the physical crosslinked CMC coating.
6) The CMC supplied by Santa Cruz Inc. failed to provide any antimicrobial activity against Gram positive *S. aureus* (ATCC 43300) and Gram negative *E. coli* (ATCC 25922) bacteria.
7) The *S. aureus* bacteria grew slower than the *E. coli* micro-organism on the same textile substrate under the same incubation conditions.
8) With respect to the "Zone of Inhibition" test method, the CMC treated samples showed no increase in their "zone of inhibition" as was expected, because there was no diffusion of the antimicrobial agent. The antimicrobial agents were crosslinked to the PET fiber surface, thus inhibiting the spread of the antimicrobial agent to the adjacent inoculated agar surface.
9) The technique described by Lamba et al provides a rapid antimicrobial assessment method for textile fabrics. For compact woven fabrics, for example, the growth of bacteria is clearly visible on the surface. However, for open and porous structures like the warp knitted mesh in this study, visualizing the bacterial growth on the fiber surface was difficult. So assessing the "growth", "reduced growth" and "no growth" classification was problematic for this type of open knitted mesh.

5.2 Future Work

- The chitosan derivative, carboxymethyl chitosan, is known to be an efficient antimicrobial agent which has been confirmed in previous work. While some parameters could affect the efficiency of the antimicrobial performance, such as molecular weight, degree of deacetylation, degree of carboxymethylation, the specific type of chitosan or chitin will determine its antimicrobial performance. The CMC in this experiment contained O-CMC with a 90% degree of deacetylation. Other chitosan derivatives are therefore recommended to be evaluated as biocompatible and safe antimicrobial agents. Obviously, a pretest of the antimicrobial activity with a minimum inhibitory concentration (MIC) assay will be necessary to determine the effectiveness and suitability of the antimicrobial agent for textile applications.

- There are other biocompatible cross-linking agents in addition to citric acid, like genipin, that will be able to crosslink chitosan derivatives. So there are other possibilities for an improved cross-linking performance in the future.

- Radio frequency atmospheric plasma treatment is known to affect the chemical properties of surfaces. An alternative type of reactive gas, such as ammonia, would provide an opportunity to activate the polyester surface with amine groups. By using a different low pressure or vacuum plasma system, more precise chemical modifications can be designed and controlled, which would make it easier to optimize surface modification for greater grafting and cross-linking efficiency.

- The quality and integrity of the CMC films attached to the PET fabric in the current study were less than perfect because the sticky CMC solution and high temperature cross-linking process led to cracking and tearing when the film samples were removed from the aluminum foil substrate after drying. An alternative approach of hanging the CMC films on a rack for high temperature crosslinking is more likely to prepare smooth and undamaged films.

- The mechanical properties of the original knitted PET structure were significantly reduced by both the CMC coating technique and the plasma treated and CMC grafting process. The cross-linking step requires exposure to an elevated temperature of 140℃ for 15 min. This temperature/ time exposure may have resulted in thermal degradation of the CMC agent, so the inclusion of an alternative lower temperature cross-linking procedure is recommended.

REFERENCES

Alonso, D., Gimeno, M., Olayo, R., Vázquez-Torres, H., Sepúlveda-Sánchez, J. D., & Shirai, K. (2009, 07). Cross-linking chitosan into UV-irradiated cellulose fibers for the preparation of antimicrobial-finished textiles. *Carbohydrate Polymers, 77*(3), 536-543.

Alves, N., & Mano, J. (2008, 12). Chitosan derivatives obtained by chemical modifications for biomedical and environmental applications. *International Journal of Biological Macromolecules, 43*(5), 401-414.

Anitha, A., Rani, V. D., Krishna, R., Sreeja, V., Selvamurugan, N., Nair, S., . . . Jayakumar, R. (2009, 11). Synthesis, characterization, cytotoxicity and antibacterial studies of chitosan, O-carboxymethyl and N,O-carboxymethyl chitosan nanoparticles. *Carbohydrate Polymers, 78*(4), 672-677.

Aubert-Viard, F., Martin, A., Chai, F., Neut, C., Tabary, N., Martel, B., & Blanchemain, N. (2015, 03). Chitosan finishing nonwoven textiles loaded with silver and iodide for antibacterial wound dressing applications. *Biomedical Materials, 10*(1), 015023.

Beard, J., Ohene-Yeboah, M., & Löfgren, J. (2016, 12). Hernia Mesh Repair and Global Surgery. *JAMA Surgery, 151*(12), 1191.

Beer, G. M., Schuster, A., Seifert, B., Manestar, M., Mihic-Probst, D., & Weber, S. A. (2009, 09). The normal width of the linea alba in nulliparous women. *Clinical Anatomy, 22*(6), 706-711.

Bhattacharya, A. (2004, 08). Grafting: A versatile means to modify polymersTechniques, factors and applications. *Progress in Polymer Science, 29*(8), 767-814.

Bhattacharya, A., Rawlins, J. W., & Ray, P. (2009). *Polymer grafting and crosslinking*. John Wiley & Sons.

Breuing, K., Butler, C. E., Ferzoco, S., Franz, M., Hultman, C. S., Kilbridge, J. F., . . . Vargo, D. (2010, 09). Incisional ventral hernias: Review of the literature and recommendations regarding the grading and technique of repair. *Surgery, 148*(3), 544-558.

Bringman, S., Conze, J., Cuccurullo, D., Deprest, J., Junge, K., Klosterhalfen, B., . . . Schumpelick, V. (2009, 12). Hernia repair: The search for ideal meshes. *Hernia, 14*(1), 81-87.

Butler, C. E., Baumann, D. P., Janis, J. E., & Rosen, M. J. (2013, 12). Abdominal wall reconstruction. *Current Problems in Surgery, 50*(12), 557-586.

Choi, C., Nam, J., & Nah, J. (2016, 01). Application of chitosan and chitosan derivatives as biomaterials. *Journal of Industrial and Engineering Chemistry, 33*, 1-10.

Cobb, W. S., Kercher, K. W., & Heniford, B. T. (2005, 03). The Argument for Lightweight Polypropylene Mesh in Hernia Repair. *Surgical Innovation, 12*(1), 63-69.

Conze, J., Kingsnorth, A. N., Flament, J. B., Simmermacher, R., Arlt, G., Langer, C., . . . Schumpelick, V. (2005). Randomized clinical trial comparing lightweight composite mesh with polyester or polypropylene mesh for incisional hernia repair. *British Journal of Surgery, 92*(12), 1488-1493.

Cooney, G. M., Lake, S. P., Thompson, D. M., Castile, R. M., Winter, D. C., & Simms, C. K. (2017, 04). The suture pullout characteristics of human and porcine linea alba. *Journal of the Mechanical Behavior of Biomedical Materials, 68*, 103-114.

Cruz, A. R., & Mautner, K. (2016, 07). Rectus Abdominis Injury in Elite Volleyball Players. *International Journal of Athletic Therapy and Training, 21*(4), 18-22.

Das, S. S. (2017). Biometrics of Pyramidalis Muscle and its Clinical Importance. *Journal Of Clinical And Diagnostic Research.*

Dastidar, T. G., & Netravali, A. N. (2012, 11). 'Green' crosslinking of native starches with malonic acid and their properties. *Carbohydrate Polymers, 90*(4), 1620-1628.

Dominguez, J. E., Gonzalez, A., & Donkor, C. (2015, 07). Robotic inguinal hernia repair. *Journal of Surgical Oncology, 112*(3), 310-314.

Dragostin, O. M., Samal, S. K., Dash, M., Lupascu, F., Pânzariu, A., Tuchilus, C., . . . Profire, L. (2016, 05). New antimicrobial chitosan derivatives for wound dressing applications. *Carbohydrate Polymers, 141*, 28-40.

Eriksen, J. R., Gögenur, I., & Rosenberg, J. (2007, 09). Choice of mesh for laparoscopic ventral hernia repair. *Hernia, 11*(6), 481-492.

Förstemann, T., Trzewik, J., Holste, J., Batke, B., Konerding, M., Wolloscheck, T., & Hartung, C. (2011, 02). Forces and deformations of the abdominal wall—A mechanical and geometrical approach to the linea alba. *Journal of Biomechanics, 44*(4), 600-606.

Gil, G., & Owski, M. (2011, 01). A New Classification of Parastomal Hernias - from the Experience at Bielański Hospital in Warsaw. *Polish Journal of Surgery, 83*(8).

Hsieh, S., Huang, Z. K., Huang, Z. Z., & Tseng, Z. S. (2004). Antimicrobial and physical properties of woolen fabrics cured with citric acid and chitosan. *Journal of Applied Polymer Science, 94*(5), 1999-2007.

Hwang, Y. J., Matthews, S., Mccord, M., & Bourham, M. (2004). Surface Modification of Organic Polymer Films Treated in Atmospheric Plasmas. *Journal of The Electrochemical Society, 151*(7).

Jiang, Q., Reddy, N., Zhang, S., Roscioli, N., & Yang, Y. (2012, 09). Water-stable electrospun collagen fibers from a non-toxic solvent and crosslinking system. *Journal of Biomedical Materials Research Part A, 101A*(5), 1237-1247.

Klinge, U., Klosterhalfen, B., Öttinger, A., Junge, K., & Schumpelick, V. (2002, 08). PVDF as a new polymer for the construction of surgical meshes. *Biomaterials, 23*(16), 3487-3493.

Korenkov, M., Paul, A., Sauerland, S., Neugebauer, E., Arndt, M., Chevrel, J., . . . Simmermacher, R. (2001, 02). Classification and surgical treatment of incisional hernia. *Langenbeck's Archives of Surgery, 386*(1), 65-73.

Lamba, N. M., Herson, D. S., Jindani, R., & King, M. W. (2017, 01). Evaluation of Antimicrobial-Treated Fabric Properties. *AATCC Journal of Research, 4*(1), 14-21.

Landuyt, K. V., Hamdi, M., Blondeel, P., & Monstrey, S. (2003, 09). The pyramidalis muscle free flap. *British Journal of Plastic Surgery, 56*(6), 585-592.

Lim, S., & Hudson, S. M. (2004, 01). Synthesis and antimicrobial activity of a water-soluble chitosan derivative with a fiber-reactive group. *Carbohydrate Research, 339*(2), 313-319.

Lovering, R. M., & Anderson, L. D. (2008, 12). Architecture and fiber type of the pyramidalis muscle. *Anatomical Science International, 83*(4), 294-297.

Mavrodin, C. I., Antoniac, V. I., & Pariza, G. (2015, 07). Relationship between Biomaterials Structure Used in Hernia Mesh Fixation and Chronic Infection. *Advanced Materials Research, 1114*, 278-282.

Miserez, M., Alexandre, J. H., Campanelli, G., Corcione, F., Cuccurullo, D., Pascual, M. H., . . . Flament, J. B. (2007, 03). The European hernia society groin hernia classication: Simple and easy to remember. *Hernia, 11*(2), 113-116.

Mishra, D., Bhunia, B., Banerjee, I., Datta, P., Dhara, S., & Maiti, T. K. (2011, 10). Enzymatically crosslinked carboxymethyl–chitosan/gelatin/nano-hydroxyapatite

injectable gels for in situ bone tissue engineering application. *Materials Science and Engineering: C, 31*(7), 1295-1304.

Morent, R., Geyter, N. D., & Leys, C. (2008, 06). Effects of operating parameters on plasma-induced PET surface treatment. *Nuclear Instruments and Methods in Physics Research Section B: Beam Interactions with Materials and Atoms, 266*(12-13), 3081-3085.

Muysoms, F. E., Miserez, M., Berrevoet, F., Campanelli, G., Champault, G. G., Chelala, E., . . . Kingsnorth, A. (2009, 06). Classification of primary and incisional abdominal wall hernias. *Hernia, 13*(4), 407-414.

Muysoms, F., Campanelli, G., Champault, G. G., Debeaux, A. C., Dietz, U. A., Jeekel, J., . . . Miserez, M. (2012, 04). EuraHS: The development of an international online platform for registration and outcome measurement of ventral abdominal wall hernia repair. *Hernia, 16*(3), 239-250.

Neděla, O., Slepička, P., & Švorčík, V. (2017, 09). Surface Modification of Polymer Substrates for Biomedical Applications. *Materials, 10*(12), 1115.

Novitsky, Y. W. (2016). *Hernia surgery: Current principles*. Springer.

Novitsky, Y. W., Elliott, H. L., Orenstein, S. B., & Rosen, M. J. (2012, 11). Transversus abdominis muscle release: A novel approach to posterior component separation during complex abdominal wall reconstruction. *The American Journal of Surgery, 204*(5), 709-716.

Pérez-Köhler, B., García-Moreno, F., Bayon, Y., Pascual, G., & Bellón, J. M. (2015, 05). Inhibition of Staphylococcus aureus Adhesion to the Surface of a Reticular Heavyweight Polypropylene Mesh Soaked in a Combination of Chlorhexidine and Allicin: An In vitro Study. *Plos One, 10*(5).

Reilingh, T. D., Geldere, D. V., Langenhorst, B., Jong, D. D., Wilt, G. V., Goor, H. V., & Bleichrodt, R. (2003, 10). Repair of large midline incisional hernias with polypropylene mesh: Comparison of three operative techniques. *Hernia, 8*(1), 56-59.

Sahariah, P., & Másson, M. (2017, 10). Antimicrobial Chitosan and Chitosan Derivatives: A Review of the Structure–Activity Relationship. *Biomacromolecules, 18*(11), 3846-3868.

Sanbhal, N., Miao, L., Xu, R., Khatri, A., & Wang, L. (2017, 01). Physical structure and mechanical properties of knitted hernia mesh materials: A review. *Journal of Industrial Textiles,* 152808371769061.

Shen, L., Xu, H., Kong, L., & Yang, Y. (2015, 08). Non-Toxic Crosslinking of Starch Using Polycarboxylic Acids: Kinetic Study and Quantitative Correlation of Mechanical Properties and Crosslinking Degrees. *Journal of Polymers and the Environment, 23*(4), 588-594.

Shin, Y., Son, K., Yoo, D. I., Hudson, S., Mccord, M., Matthews, S., & Whang, Y. (2006). Functional finishing of nonwoven fabrics. I. Accessibility of surface modified PET spunbond by atmospheric pressure He/O2 plasma treatment. *Journal of Applied Polymer Science, 100*(6), 4306-4310.

Simoncic, B., & Tomsic, B. (2010, 03). Structures of Novel Antimicrobial Agents for Textiles - A Review. *Textile Research Journal, 80*(16), 1721-1737.

Śmietański, M., Szczepkowski, M., Alexandre, J. A., Berger, D., Bury, K., Conze, J., . . . Muysoms, F. (2013, 10). European Hernia Society classification of parastomal hernias. *Hernia, 18*(1), 1-6.

Strain, I. N., Wu, Q., Pourrahimi, A. M., Hedenqvist, M. S., Olsson, R. T., & Andersson, R. L. (2015). Electrospinning of recycled PET to generate tough mesomorphic fibre membranes for smoke filtration. *Journal of Materials Chemistry A, 3*(4), 1632-1640.

Upadhyaya, L., Singh, J., Agarwal, V., & Tewari, R. P. (2013, 01). Biomedical applications of carboxymethyl chitosans. *Carbohydrate Polymers, 91*(1), 452-466.

Urquhart, D. M., Barker, P. J., Hodges, P. W., Story, I. H., & Briggs, C. A. (2005, 03). Regional morphology of the transversus abdominis and obliquus internus and externus abdominis muscles. *Clinical Biomechanics, 20*(3), 233-241.

Wang, X., Du, Y., Luo, J., Yang, J., Wang, W., & Kennedy, J. F. (2009, 07). A novel biopolymer/rectorite nanocomposite with antimicrobial activity. *Carbohydrate Polymers, 77*(3), 449-456.

Wang, X., Han, C., Hu, X., Sun, H., You, C., Gao, C., & Haiyang, Y. (2011, 10). Applications of knitted mesh fabrication techniques to scaffolds for tissue engineering and regenerative medicine. *Journal of the Mechanical Behavior of Biomedical Materials, 4*(7), 922-932.

Wang, Y., & Zhang, P. (2014, 03). A comparative study of polyvinylidene fluoride and polypropylene hernia meshes in creep behavior and elasticity. *Textile Research Journal, 84*(14), 1558-1566.

Widsten, P., Dooley, N., Parr, R., Capricho, J., & Suckling, I. (2014, 01). Citric acid crosslinking of paper products for improved high-humidity performance. *Carbohydrate Polymers, 101*, 998-1004.

Xie, L., Jiao, L., & Dai, H. (2010, 10). Selective Etching of Graphene Edges by Hydrogen Plasma. *Journal of the American Chemical Society, 132*(42), 14751-14753.

Yadav, H. K., & Shivakumar, H. G. (2012). In Vitro and In Vivo Evaluation of pH-Sensitive Hydrogels of Carboxymethyl Chitosan for Intestinal Delivery of Theophylline. *ISRN Pharmaceutics, 2012,* 1-9.

Yu, L. Y., Zhu, B., Cai, X., Wang, Y. W., Han, R. H., & Li, Y. W. (2016, 04). Review of Polymer Surface Modification Method. *Materials Science Forum, 852,* 626-631.

Zöller, B., Ji, J., Sundquist, J., & Sundquist, K. (2013, 08). Shared and Nonshared Familial Susceptibility to Surgically Treated Inguinal Hernia, Femoral Hernia, Incisional Hernia, Epigastric Hernia, and Umbilical Hernia. *Journal of the American College of Surgeons, 217*(2).